3160-08

INTERACTIONS OF STRESS WAVES WITH CRACKS IN ROCK MEDIA

Mark H. Wagner
Paul J. Blatz

SEMI-ANNUAL REPORT

September 1971

Sponsored by

Advanced Research Projects Agency
ARPA Order No. 1597, Amend. 2
Program Code 1F10

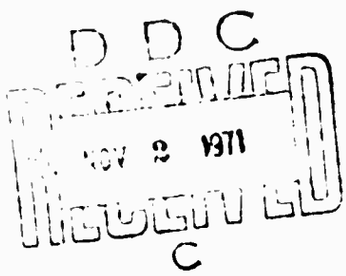

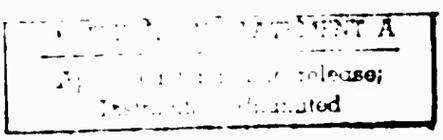

Prepared by

SHOCK HYDRODYNAMICS INCORPORATED
A Subsidiary of the Whittaker Corporation
15010 Ventura Boulevard
Sherman Oaks, California 91403

DOCUMENT CONTROL DATA - R & D

(Security classification of title, body of abstract and indexing annotation must be entered when the overall report is classified)

1 ORIGINATING ACTIVITY (Corporate author)
SHOCK HYDRODYNAMICS INCORPORATED
15010 Ventura Boulevard
Sherman Oaks, California 91403

2a. REPORT SECURITY CLASSIFICATION
UNCLASSIFIED

2b. GROUP
N/A

3 REPORT TITLE

INTERACTIONS OF STRESS WAVES WITH CRACKS IN ROCK MEDIA

4 DESCRIPTIVE NOTES (Type of report and inclusive dates)
Semi-Annual, 25 January 1971 - 25 July 1971

5. AUTHOR(S) (First name, middle initial, last name)
Mark H. Wagner
Paul J. Blatz

6 REPORT DATE	7a. TOTAL NO OF PAGES	7b. NO OF REFS
September 1971	67	11

8a. CONTRACT OR GRANT NO.	9a. ORIGINATOR'S REPORT NUMBER(S)
H0210019	
b. PROJECT NO. ARPA Order No. 1597, Amend. 2	3160-08
c. Program Code 1F10	9b. OTHER REPORT NO(S) (Any other numbers that may be assigned this report)
d.	

10. DISTRIBUTION STATEMENT

Distribution of this document is unlimited.

11 SUPPLEMENTARY NOTES	12. SPONSORING MILITARY ACTIVITY
This contract is monitored by the Bureau of Mines.	Advanced Research Projects Agency

13 ABSTRACT

Two-dimensional numerical solutions of three problems of stress wave interactions with oblique cracks in granite have been carried out using the SHEP code, a finite-difference Lagrangian program that incorporates a comprehensive hydrodynamic-elastic-plastic behavioral model. The problems involve both infinite and finite-length crack surfaces. To enable the study of propagation of cracks under stress wave loading, a dynamic Griffith criterion has been formulated for incorporation into the code. Comparisons of the numerical results with analytic solutions for model problems are being obtained to verify the code. Included in these correlations is the problem of an accelerating crack for the case of anti-plane shear.

DD FORM 1 NOV 65 1473

14 KEY WORDS	LINK A		LINK B		LINK C	
	ROLE	WT	ROLE	WT	ROLE	WT
Wave Propagation						
Crack Propagation						
Fracture						
Rock Mechanics						
Two-Dimensional Numerical Techniques						

3160-08

INTERACTIONS OF STRESS WAVES WITH CRACKS IN ROCK MEDIA

Mark H. Wagner
Paul J. Blatz

SEMI-ANNUAL REPORT

September 1971

Sponsored by
Advanced Research Projects Agency
ARPA Order No. 1597, Amend. 2

Program Code 1F10

This research was supported by the Advanced Research Projects Agency of the Department of Defense and was monitored by the Bureau of Mines under Contract No. H0210019.

Principal Investigators: M. H. Wagner/P. J. Blatz (213) 783-7210
Project Officer: T. E. Ricketts (612) 725-4608

Effective Date of Contract: 25 January 1971
Contract Expiration Date: 25 February 1972
Amount of Contract: $61,387

Prepared by

SHOCK HYDRODYNAMICS INCORPORATED
A Subsidiary of the Whittaker Corporation
15010 Ventura Boulevard
Sherman Oaks, California 91403

ABSTRACT

Two-dimensional numerical solutions of three problems of stress wave interactions with oblique cracks in granite have been carried out using the SHEP code, a finite-difference Lagrangian program that incorporates a comprehensive hydrodynamic-elastic-plastic behavioral model. The problems involve both infinite and finite-length crack surfaces. To enable the study of propagation of cracks under stress wave loading, a dynamic Griffith criterion has been formulated for incorporation into the code. Comparisons of the numerical results with analytic solutions for model problems are being obtained to verify the code. Included in these correlations is the problem of an accelerating crack for the case of anti-plane shear.

TABLE OF CONTENTS

TABLE OF CONTENTS (Cont'd)

1. INTRODUCTION

The objective of this program is to apply two-dimensional numerical techniques to the solution of problems of stress wave interactions with individual, oblique cracks in rock media. Computer codes suitable for solving a wide range of fluid and solid mechanics problems have been available or under development for several years and efforts to extend these techniques to the quantitative analysis of wave interactions with cracks and of crack motion are now feasible. Shock Hydrodynamics two-dimensional SHEP (Shock Hydrodynamic Elastic Plastic) code is being utilized for this purpose in this program.

This report describes the work conducted during the first six months of the program.

2. SUMMARY

2.1 PROBLEM AREA

Excavation processes in rock media typically involve the action of strong dynamic stresses introduced either from explosive, mechanical, or other impulsive loading sources. The propagation of stress waves in homogeneous, isotropic media is reasonably well understood. In-situ rock media, however, typically contain large scale discontinuities in the form of cracks, joints, and faults. Interactions of stress waves with these discontinuities can cause slippage along the cracks, or extension (propagation) of the cracks, or separation. The interactions can also alter the characteristics of the stress wave transmitted across the discontinuity.

This study is concerned with an analysis of the detailed mechanisms involved when strong stress waves interact with the crack surfaces in jointed block media. Of particular interest are cracks which are obliquely oriented relative to the wave front. The understanding thus obtained can contribute to the advancement of knowledge of excavation processes in various media, and how to control and/or improve such processes.

The technical approach that is being used in studying the details of stress wave-crack interactions is based on two-dimensional numerical analyses of the dynamic phenomena occurring under various conditions of stress wave profile, crack orientation relative to the wave front, and degree of locking (or lubrication) initially found across the crack. The computer program being used to obtain the numerical solutions is the SHEP code. SHEP is a finite-difference Lagrangian program employing a comprehensive hydrodynamic-elastic-plastic behavioral model. SHEP has been under intensive use and development for the past six years and has been applied to a broad spectrum of wave propagation problems.

A major difficulty in examining wave interactions with discontinuities such as cracks or fracture surfaces arises due to the constraint of the continuum model which is normally assumed in numerical analyses of wave propagation. Special routines in the SHEP code alleviate this difficulty by permitting crack surfaces to be explicitly defined in the computational grid. Thus the grid is not coupled across the crack, and slippage and/or separation can occur.

2.2 PLAN OF RESEARCH

The work under the current contract is divided into the following two tasks, corresponding to analyses of stress wave interactions with

a) single, infinite cracks and
b) single, finite-length cracks.

2.2.1 Task 1 - Interaction of Stress Waves with Single, Infinite Cracks

This task is concerned with the analysis pertaining to cracks which are infinite in extent, or which intersect with the ground surface. The work initially consists of the selection and determination of the problem specifications (such as media properties, loading wave characteristics, and crack orientation and condition). SHEP code solutions of the problems defined are then set up and run. These solutions provide complete quantitative data for

all the state and motion variables of interest throughout the computing field at regular intervals of time. In addition, spatial plots of the principal stress, particle velocity, and displacement fields are obtained at selected times during the event. Following completion of the solutions, analysis and interpretation of the results are performed to assess the important mechanisms and factors influencing the behavior of the crack and the characteristics of the transmitted stress wave.

2.2.2 Task 2 - Interaction of Stress Waves with Single, Finite Cracks

This task is similar to Task 1, except that the class of cracks involved are those of finite length, so that the interaction of a stress wave with a crack tip can be examined. Particular attention is being given to the stress magnitudes developed near the tip, and the effect of the tip on the transmitted wave system. The problems are selected so that comparisons between the cases of infinite (Task 1) and finite (Task 2) cracks can be made.

Also included in this task is the development of a dynamic Griffith criterion to be incorporated into the code for the study of crack propagation under stress wave loading.

To verify the suitability and accuracy of the code, and modifications made thereto during the course of the program, for analyses of wave/crack interactions, analytic solutions of selected test problems are being obtained and used to check-out corresponding numerical solutions obtained with the code.

2.3 MAJOR ACCOMPLISHMENTS

Primary program accomplishments during this period included

a) The completion of three SHEP code solutions of stress wave/crack interaction problems,
b) the initial formulation of a dynamic Griffith criterion for crack propagation, suitable for incorporation into the code, and

c) the initiation of a series of test cases to verify the numerical results through comparison with analytic solutions that are being obtained.

2.3.1 Numerical Solutions

Three problems of wave interactions with cracks were selected for analysis by means of code solution, as depicted in Figure 1. These problems were chosen to demonstrate the utility of numerical techniques for obtaining detailed information on the response of cracked media subjected to impulsive loads, in general, and, in particular, for assessments of the wave interactions in the vicinity of a crack. It is noted that the explicit definition of a crack surface such as specified in these problems is not generally amenable to treatment through conventional code techniques, which normally assume a continuous material model.

The rock medium selected for these problems was granite. The material properties assumed for the granite are described in Section 3.2 of this report. The problems were run in plane geometry, assuming plane strain; the variables are thus independent of the z-coordinate (perpendicular to the cross-section shown).

The first problem selected for analysis (Case 1) consisted of interactions of a stress wave with a crack oriented at a 30° angle with the wave front. The stress wave was generated by uniformly loading the left face of the granite block with a pressure pulse. A triangular pressure pulse of 5 kilobars peak magnitude and 0.2 millisecond duration was used for this problem, as sketched below:

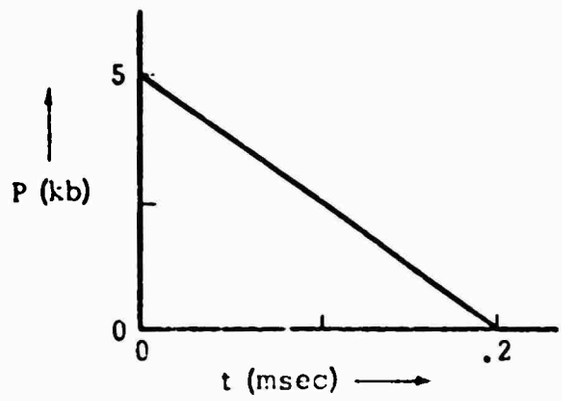

CASE 1. INTERACTION OF STRESS WAVE WITH SINGLE, INFINITE CRACK

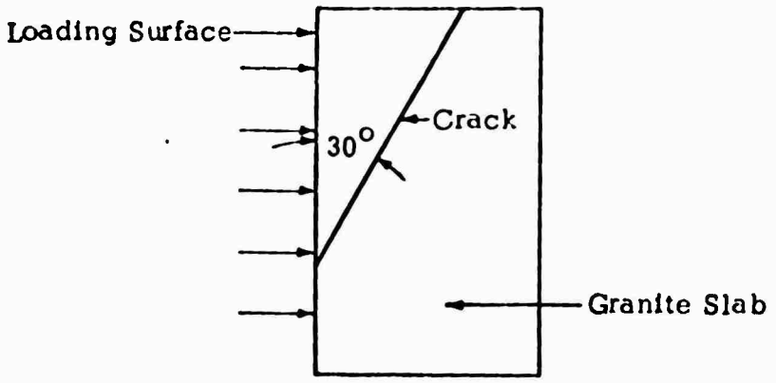

CASE 2. INTERACTION OF STRESS WAVE WITH SINGLE, FINITE-LENGTH CRACK

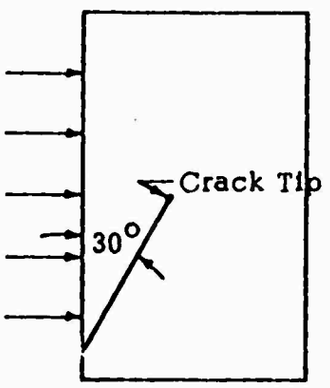

CASE 3. INTERACTION OF STRESS WAVE WITH SINGLE, FINITE-LENGTH CRACK, WITH CRACK GROWTH

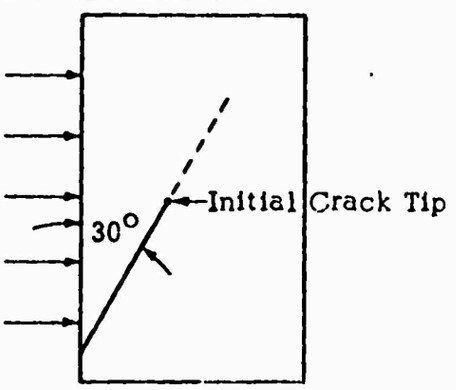

Figure 1. Specifications of Problems for SHEP Code Solutions.

The crack in this problem was characterized by a free slip condition and zero width. Opening of the crack was allowed to occur if stress components normal to the crack went into tension.

The second problem considered (Case 2) involved the interaction of a stress wave with a finite-length crack. The angle of orientation of the crack and the applied pressure loading were the same as in the first problem. The crack extended from the loading surface (lower left) to the crack tip, situated on the horizontal mid-plane of the block.

Case 3 was the same as the second problem, except that crack growth was permitted. This case demonstrates the provisions in the code which can be used to model crack propagation. In this case, dynamic decoupling of lattice points in the computing mesh occurs when a specified criterion is satisfied.

SHEP code solutions of these three problems were successfully completed. Plots depicting the particle velocity field and the principal stress field occurring in the test block were obtained for several times during the interactions. In addition, time histories of pertinent parameters at several stations in the field were recorded. These results are discussed in detail in Section 3 of the report. Some representative results of these code solutions are shown here, in Figures 2 to 7.

For Case 1, the principal stress field, for a time of .3 msec, and the particle velocity field, for a time of .5 msec, are shown in Figures 2 and 3. As the wave encounters the crack, the principal stress vectors may be seen (Figure 2) to rotate into a direction transverse to the crack surface, reflecting the fact that the crack surface can not bear shear stress. This interaction produces a dilatational wave and trailing shear wave which propagate across the block, as indicated in the velocity field plot (Figure 3). The peak stress in the transmitted wave was reduced by about 25% from that in the incident wave.

An example of the results of the Case 2 solution is shown in Figure 4, which depicts the particle velocity field occurring at a time of .6 msec. In this interaction, the wave system is divided approximately in

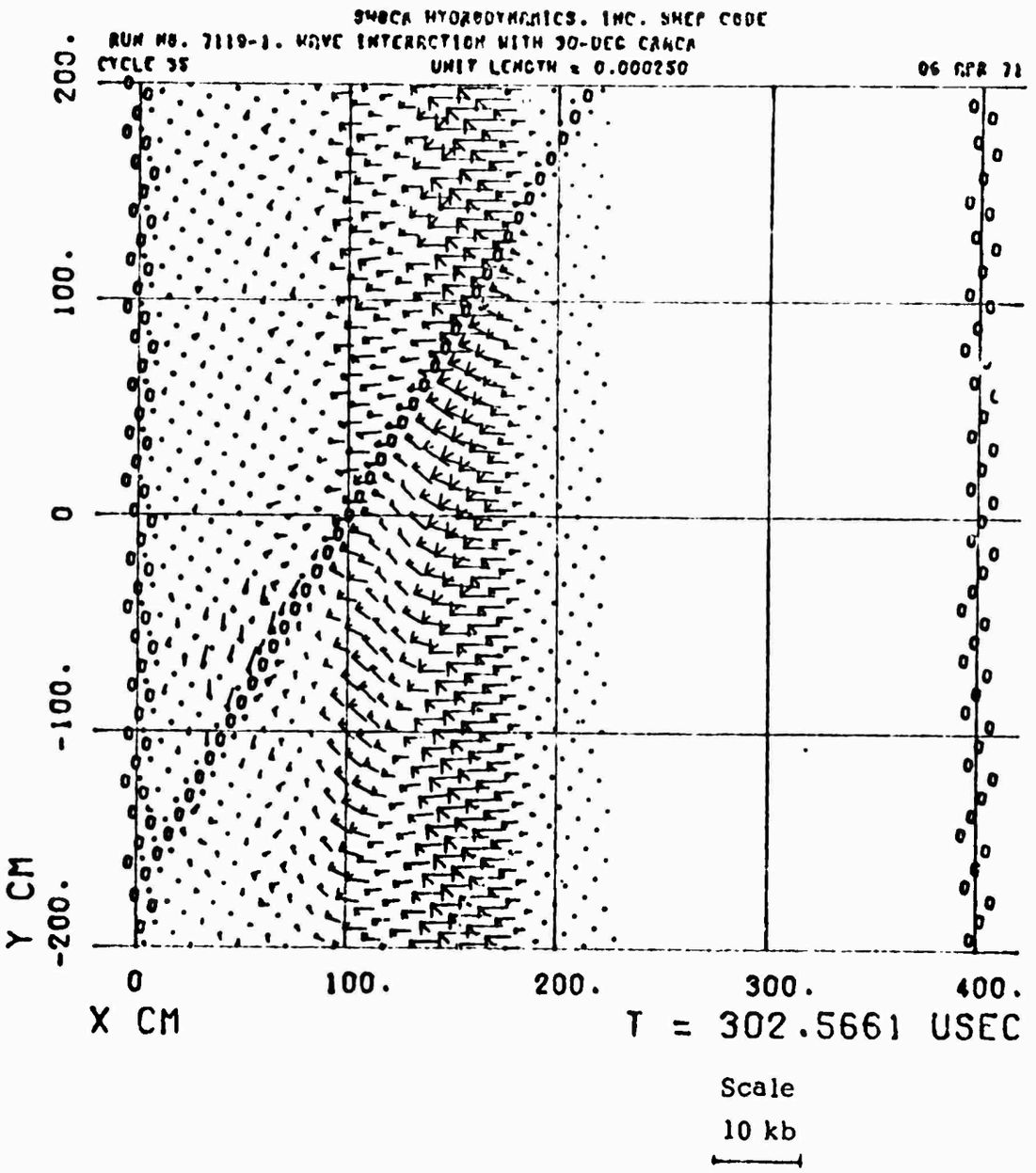

Figure 2. Principal Stress Field, Case 1

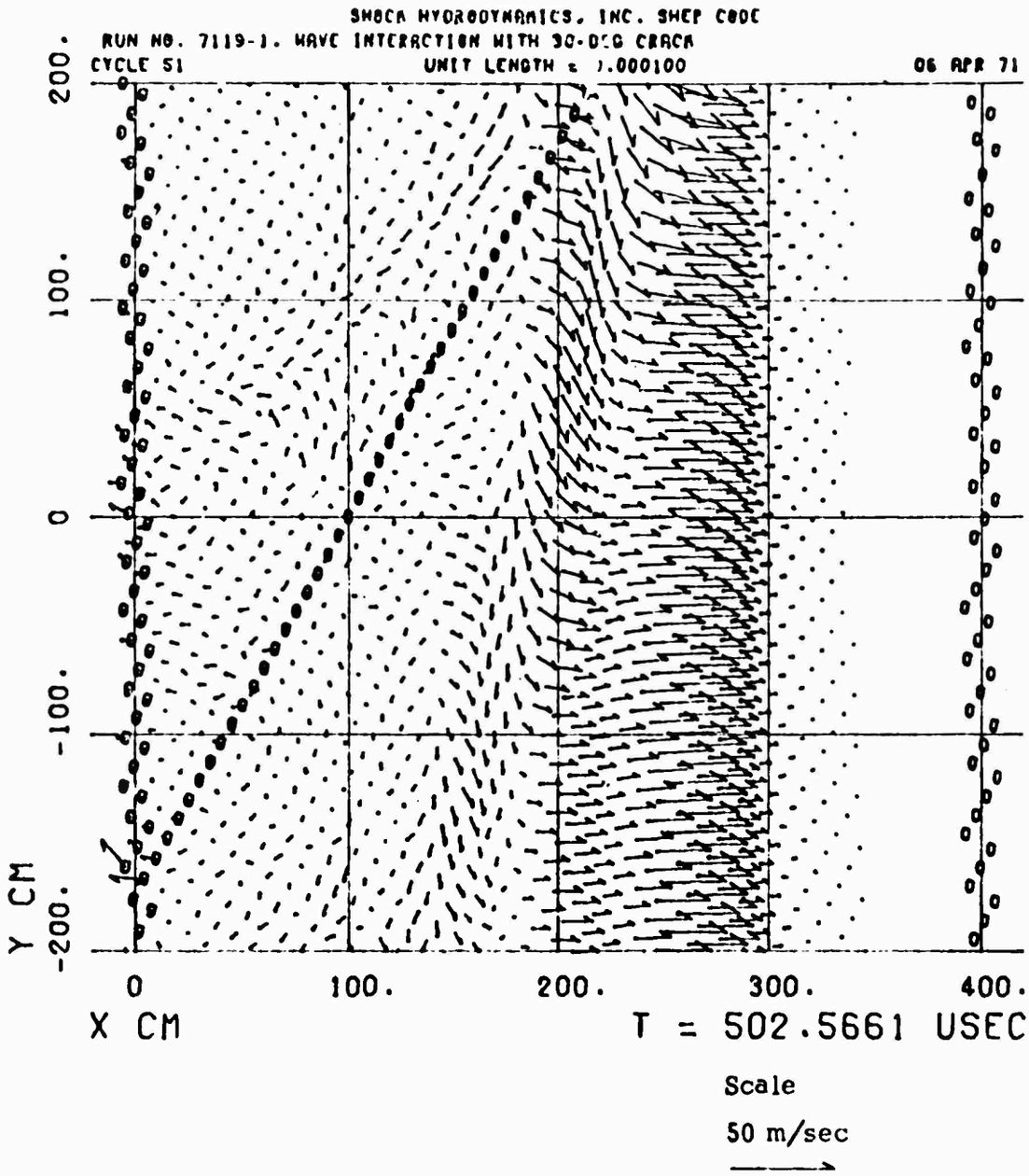

Figure 3. Particle Velocity Field, Case 1

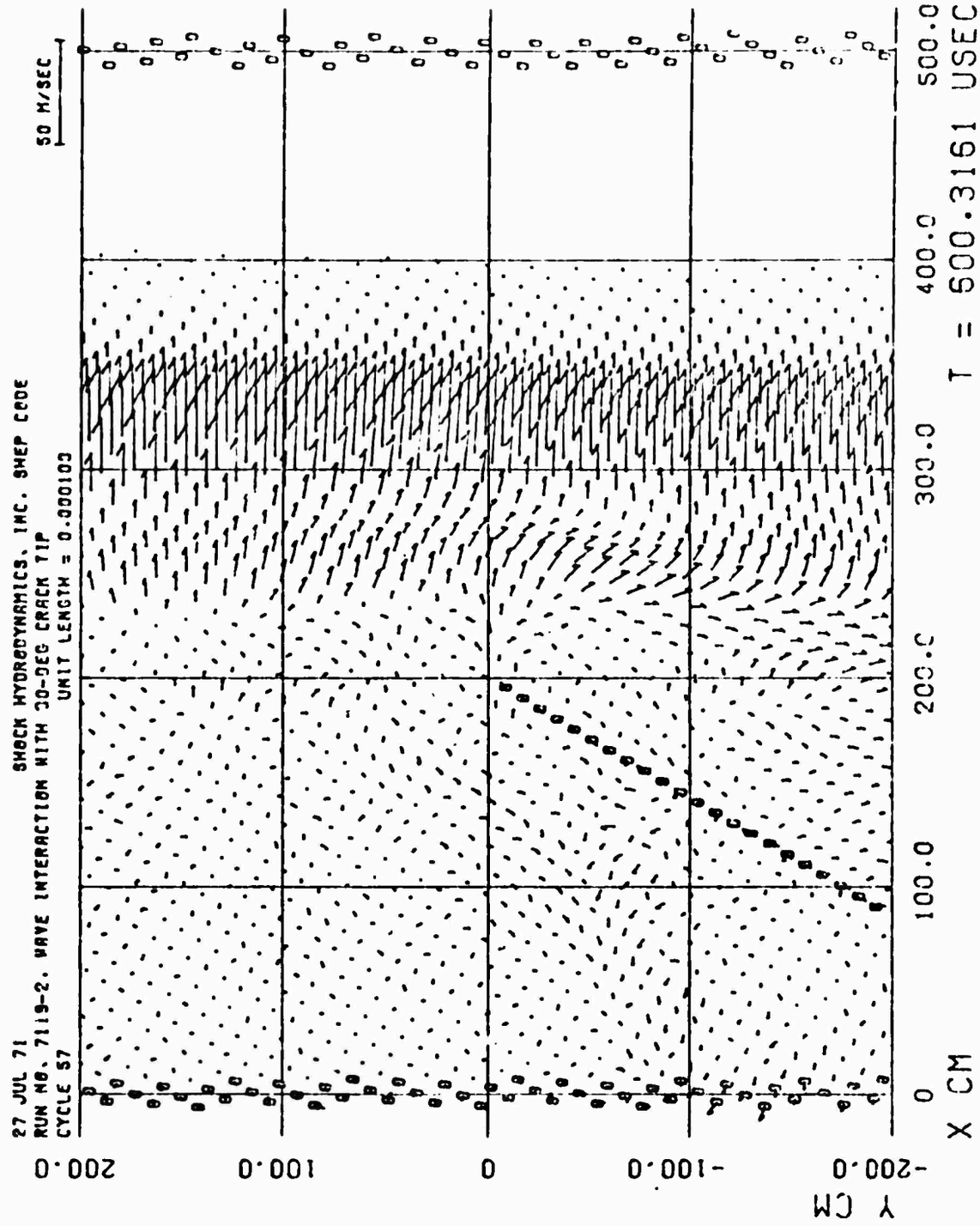

Figure 4. Particle Velocity Field, Case 2.

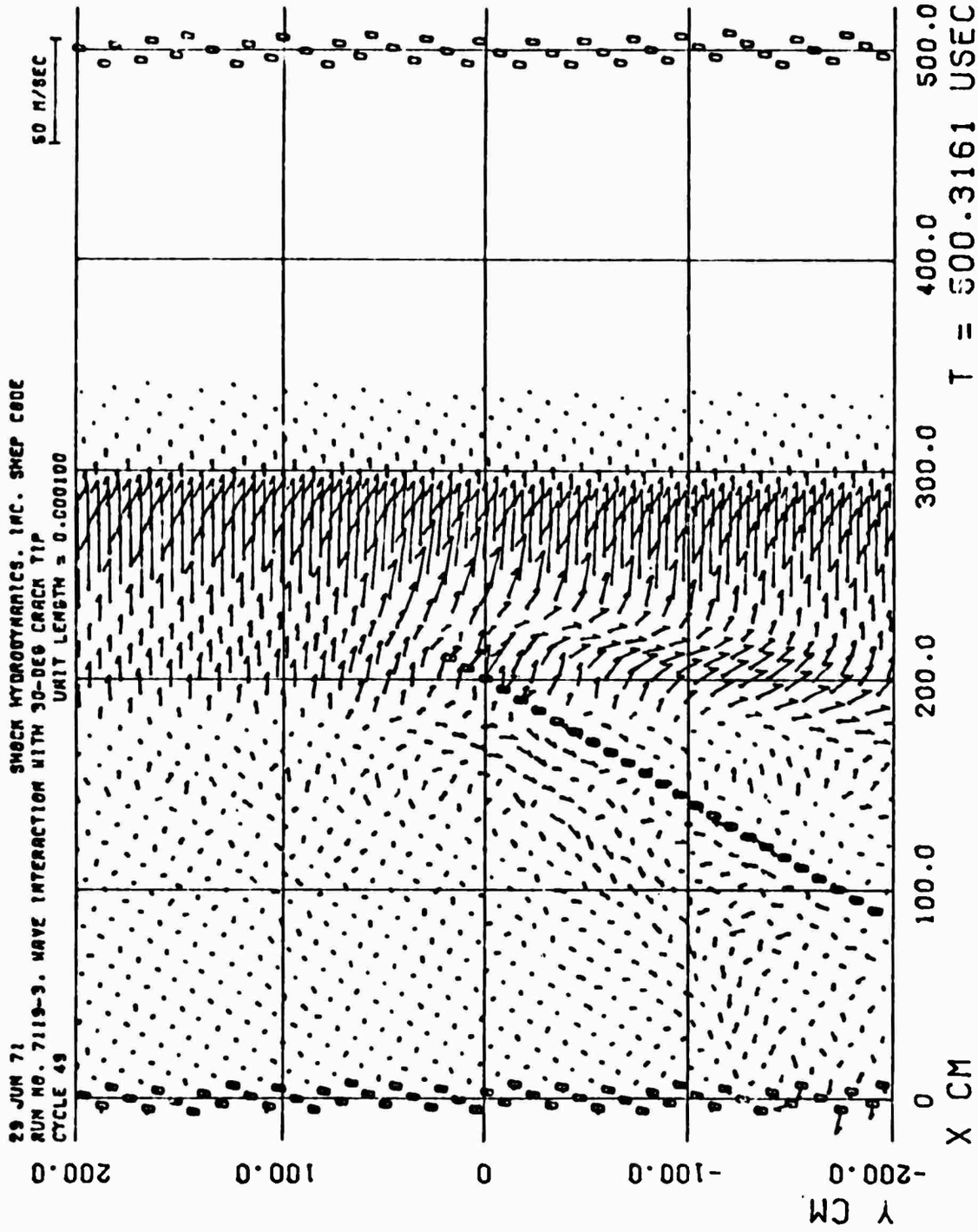

Figure 5. Particle Velocity Field, Case 3.

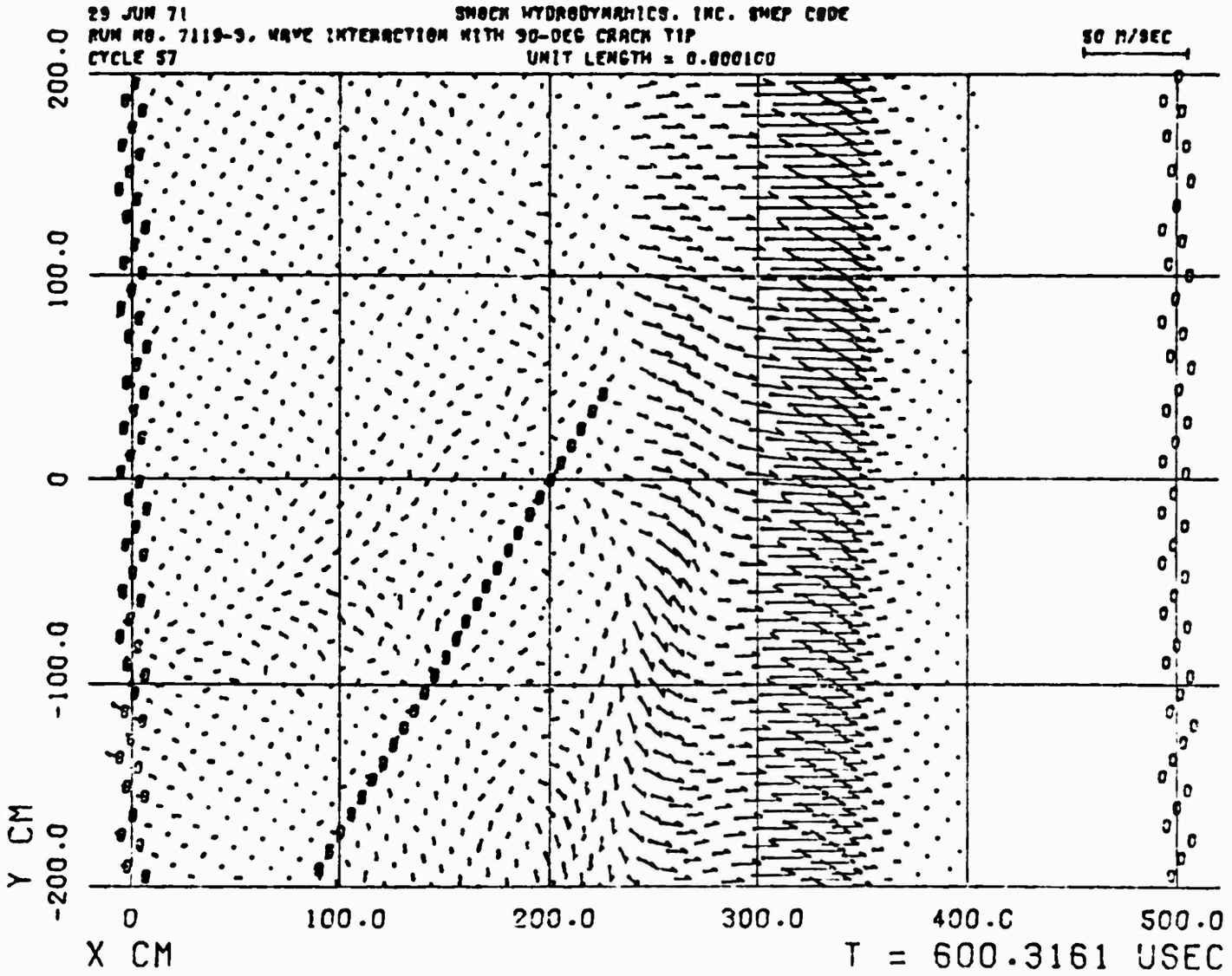

Figure 6. Particle Velocity Field, Case 3.

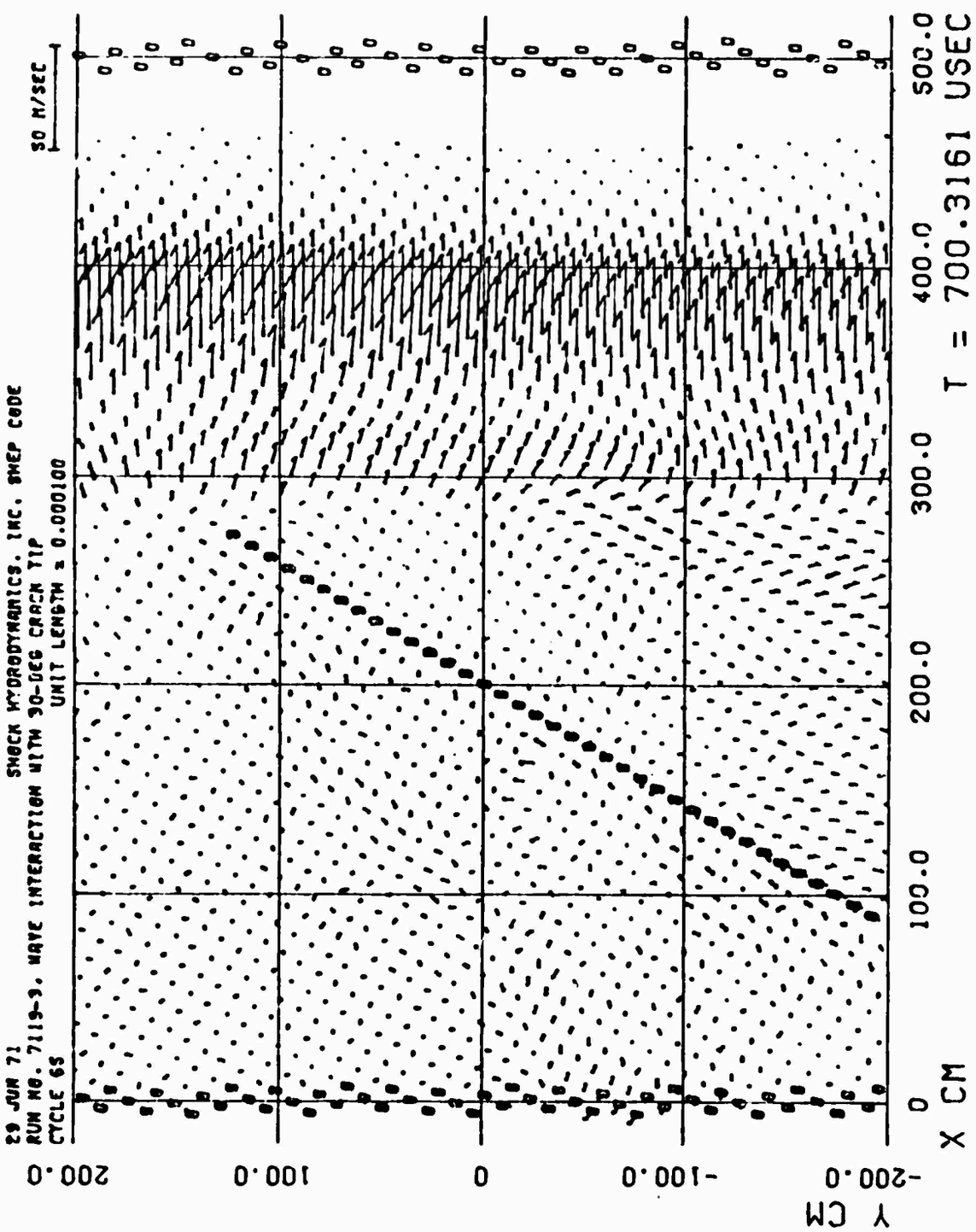

Figure 7. Particle Velocity Field, Case 3.

half, the part above the crack tip appearing as a simple plane wave, and that below as a dilatational wave and trailing shear wave, as in the previous solution. Starting from the crack tip, a disturbance propagates into the plane wave region above and the "cracked" region below, altering both flow fields and creating an expanding region of transition between them.

In Case 3, where crack growth was allowed, the criterion used for decoupling of points beyond the crack tip was that each of the cells surrounding a lattice point must have failed, i.e., at some time reached a state on the granite failure surface. This was a conservative criterion, since the failure surface generally represents states where virtually complete fracture occurs. Use of more sensitive criteria can be employed, and development of a dynamic Griffith criterion is currently under development, as described below. The crack growth occurring in this solution is indicated in Figures 5, 6, and 7, which are plots of the particle velocity field for times of .5, .6, and .7 msec. The extent of the crack in each plot is indicated by the circled lattice points.

2.3.2 Dynamic Griffith Criterion

In connection with efforts being made under the program to enable the study of propagation of cracks under stress wave loading, the incorporation of equations into the SHEP code which govern the rate of propagation of a brittle crack surface in an elastic material is currently under development. These equations are known as the Griffith criterion and they provide a relation between power input to the body and the rate of uptake of this power by strain energy, kinetic energy, and new surface energy. The concept of surface energy is the feature that was introduced by Griffith in the early 1900's, and it requires the determination of an additional material parameter, namely the surface energy per unit area. It is planned to extract the value of this parameter for granite from available fracture data.

2.3.3 Analytical Comparison Problems

To verify the SHEP code solutions and the formulation changes being made, comparisons of numerical results with analytical solutions of model problems are being made.

As part of this effort, the capability has been added to the code for the treatment of anti-plane shear, or out-of-plane displacements, with the restriction that the motions are independent of the z-coordinate, so as to retain the two-dimensional character of the code. This was done primarily since the only elasto-dynamic solutions currently available for an accelerating crack are those for the case of anti-plane shear, although it also represents a useful tool in numerical analysis which has heretofore been unavailable.

A model problem of simple, shear motion of a slab has been solved with the modified code. The results of the code solution showed excellent agreement with the analytical solution for this case. The next case in this series, currently in work, is a problem involving the interaction of an anti-plane shear wave with a stationary crack.

3. NUMERICAL SOLUTIONS

As noted above, numerical solutions of three problems involving the interaction of stress waves with cracks were performed. The specifications of these problems were given in Section 2.3.1.

3.1 COMPUTATIONAL METHOD

3.1.1 Physical Model

The computer program being used in this study is the two-dimensional SHEP code, which solves the equations of motions for elastic-plastic bodies by means of a finite-difference Lagrangian-cell technique. SHEP has been under intensive use and development for the past six years and has been previously documented[1] and distributed to interested parties. The mathematical formulation is basically the same as that described by Wilkins[2]. To

delineate the boundary between elastic and plastic deformations, various yield criteria may be used, such as von Mises, Mohr-Coulomb, or arbitrary functions. Within the chosen yield surface, the deformations are considered to be elastic, i.e., when

$$\sqrt{3 J_2'} < Y \tag{1}$$

where J_2' is the second invariant of the deviatoric stress tensor and Y is the yield strength. Excursions on the yield surface are made in accordance with the Prandtl-Reuss flow rule.

To model a crack surface, SHEP contains provisions for inserting surfaces of discontinuity, which consist of grid lines having a dual set of lattice points. These surfaces are discussed in the following section.

3.1.2 Surfaces of Discontinuity

In a normal Lagrangian computational grid, material elements on either side of an interface at any point are coupled to each other for the entire problem; they are, i.e., locked or welded together along the line segment connecting any two lattice points along the interface. At any interface, which may represent a crack within a material or the boundary between two different materials, there are, however, in general, special boundary conditions which apply, and, in addition, there is the possibility of forces which may be set up that tend to cause the materials to slip past each other or to separate. A gas flowing past a metal surface is an example of such a case. The onset of material fracture during a problem also gives rise to the requirement for treating the decoupling or uncoupling of elements which are, in this case, within an originally competent material. For application to problems in fracture mechanics, such as in this program, the latter requirement is particularly important.

A formulation of sliding interfaces for Lagrangian codes, as reported by Wilkins[2], provided a capability for the numerical treatment of problems involving sliding of two materials along an interface. This formulation served as the basis for development of the surface of discontinuity capability currently available in the SHEP code.

The basic features of the surface of discontinuity formulation are illustrated in Figure 8. The grid line corresponding to the surface of discontinuity is known in common parlance as a slide line. At the start of a problem, the lattice points along the slide line may be individually designated as decoupled points, corresponding to their lying on an interface, or as coupled points, in which case their behavior is the same as in an ordinary mesh. For decoupled points, special sets of governing equations are used to individually determine the motion of the point pairs, to reflect the fact that there is an interface, such that, e.g., shear stress cannot be supported. If forces are present which tend to cause slippage, the decoupled points will thus disengage and move separately along the slide line.

Additionally, the development of tensile stresses normal to an interface will tend to cause material separation and formation of voids. Provisions have been made in the code to treat this phenomenon, also.

The void opening test is made by computing the stress normal to the interface at a decoupled slide point and comparing this value with a selected critical value of stress required for uncoupling. If the computed stress is greater than the critical value (in tension), then that point is designated as a free surface point. The newly formed free point is then moved in accordance with the regular equations of motion for a point on a free surface.

For the problems performed in this study, the critical value for uncoupling was set to zero, such that any tensile stress would tend to cause separation. In other applications, e.g., for the interfaces in laminated materials, this value could be set equal to the bond strength.

Void closure may also occur and is treated in the code by appropriate tests to determine if the materials have come in contact. If so, the equations of the surface of discontinuity are restored, and the materials may subsequently slip or re-open, as before.

Lattice points along the slide line which are initially designated as coupled points may dynamically decouple, individually, during the course of a problem, if a selected criterion is met. Various decoupling,or fracture, criteria may be used. Once the lattice points are decoupled, the equations

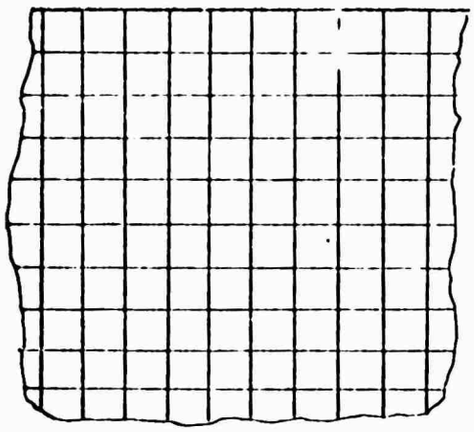

a. Normal Coupled Lagrangian Grid

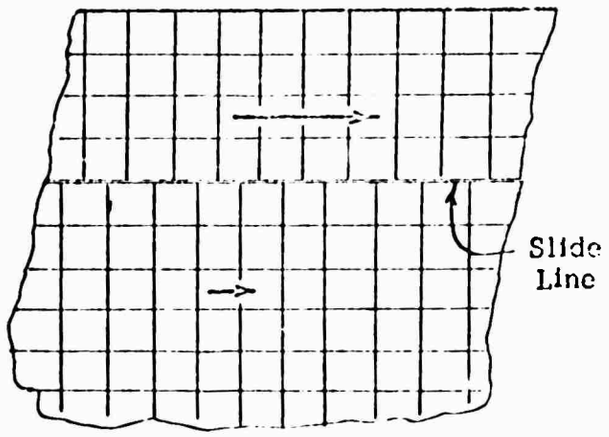

b. Decoupled Grid With Relative Motion (Slippage) Along Material Interface, Fracture Surface, or Plane of Weakness

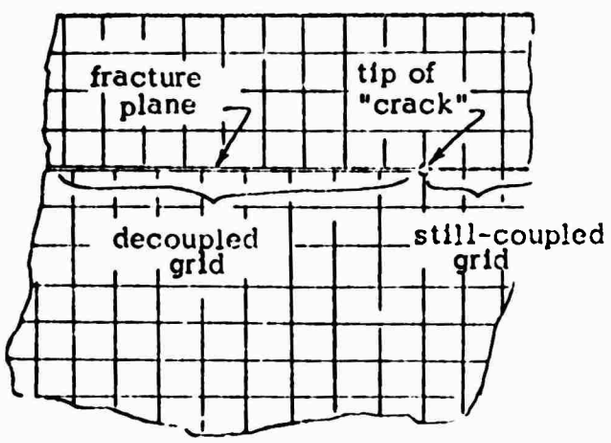

c. "Crack Propagation" With Subsequent Slippage Along Fracture Surface

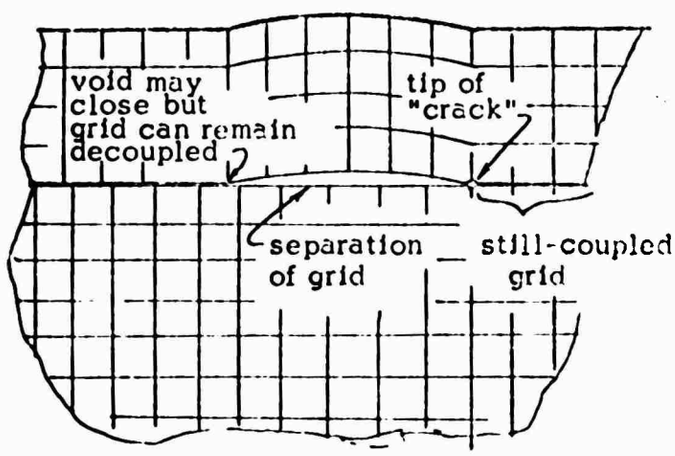

d. "Crack Propagation" With Subsequent Separation and Rejoining Along Fracture Surface

Figure 8. Schematic Illustrations of the Treatment of Slippage, Fracture, Void Opening, and Void Closing Along Surfaces of Discontinuity in the SHEP Code.

of the surface of discontinuity are invoked. A mechanism is thus provided which can be used to model crack propagation within a material.

Additional information on the code operations and the mathematical basis of sliding interfaces has been previously reported.[2-4]

3.2 MATERIAL PROPERTIES

The rock medium in these problems was granite. The properties selected for the granite were:

Density:	$\rho_o = 2.69$ gm/cm^3
Dilatational Velocity:	$v_{d_o} = .579$ cm/μsec
Shear Velocity:	$v_{s_o} = .330$ cm/μsec

These values imply the following other properties:

Bulk Modulus:	$K_o = .512$ Mb
Shear Modulus:	$G_o = .293$ Mb
Poisson's Ratio:	$\nu_o = .26$

The subscript o in the above indicates that these are normal, pre-shocked values. These values were selected from previous studies involving granite media (References 5 and 6).

The equation of state of granite, suitable for the low-pressure regime applicable in these problems, was formulated as follows.

$$P = A\mu + B\mu^2\delta + G\rho e \qquad P < .04 \text{ Mb} \qquad (2)$$

where

$\delta = 1$ for $\mu > 0$

$\delta = 0$ for $\mu \leq 0$

The symbols are defined as

e = specific internal energy

P = pressure

$\eta = \rho/\rho_o$ = relative density

$\mu = \eta - 1$ = compression

ρ = density

The values of the coefficients are:

A = .512 Mb

B = 1.49 Mb

G = 2.1

No hydrostatic tension was permitted, i.e., $P_{min} = 0$.

A Mohr-Coulomb type yield model was used, i.e.,

$$Y = .0003 + (1-e^{-P/.0003})(.00094 + 1.33\ P) \qquad (3)$$

where Y is the yield strength, in megabars. The maximum value permitted for Y was 10 kilobars.

3.3 CASE 1 - INTERACTION OF STRESS WAVE WITH SINGLE, INFINITE CRACK

The computational grid set up for the code solution of Case 1 is shown in Figure 9. This grid contains 2690 cells, with the basic cell size set at 10 cm x 10 cm. Beyond a central region of interest the cell dimensions geometrically increase in order to conserve the total cell count and computational time. Representative results of the code solution, as depicted by particle velocity fields and/or principal stress fields for times of .3, .5, and .92 msec, are shown in Figures 10 to 12 and in Figures 2 and 3 in the Summary, Section 2.3.1. For clarity in reading these plots, the field of view was limited to the central region of interest.

For the stress field plots, the principal components of the stress tensor for each cell are shown, as follows: The magnitude of the two principal stresses in the x-y plane are plotted in their corresponding principal directions. The third principal stress (in the z direction) is plotted along the line bisecting the other two principal directions. Vectors pointing to the right are compressive, to the left, tensile. An example of how a stress tensor is plotted is sketched below:

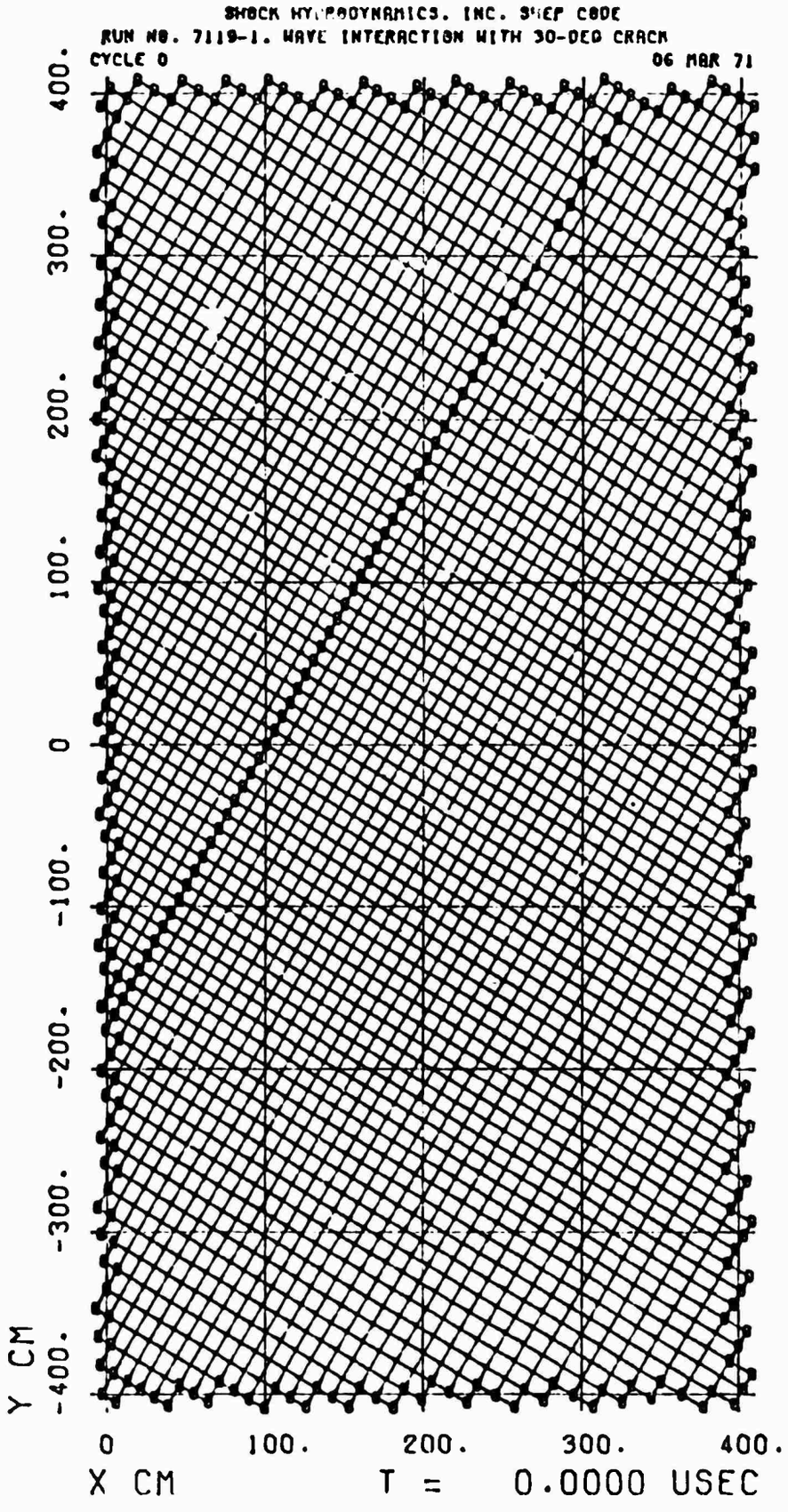

Figure 9. Initial Configuration of the Lagrangian Computational Grid, Case 1

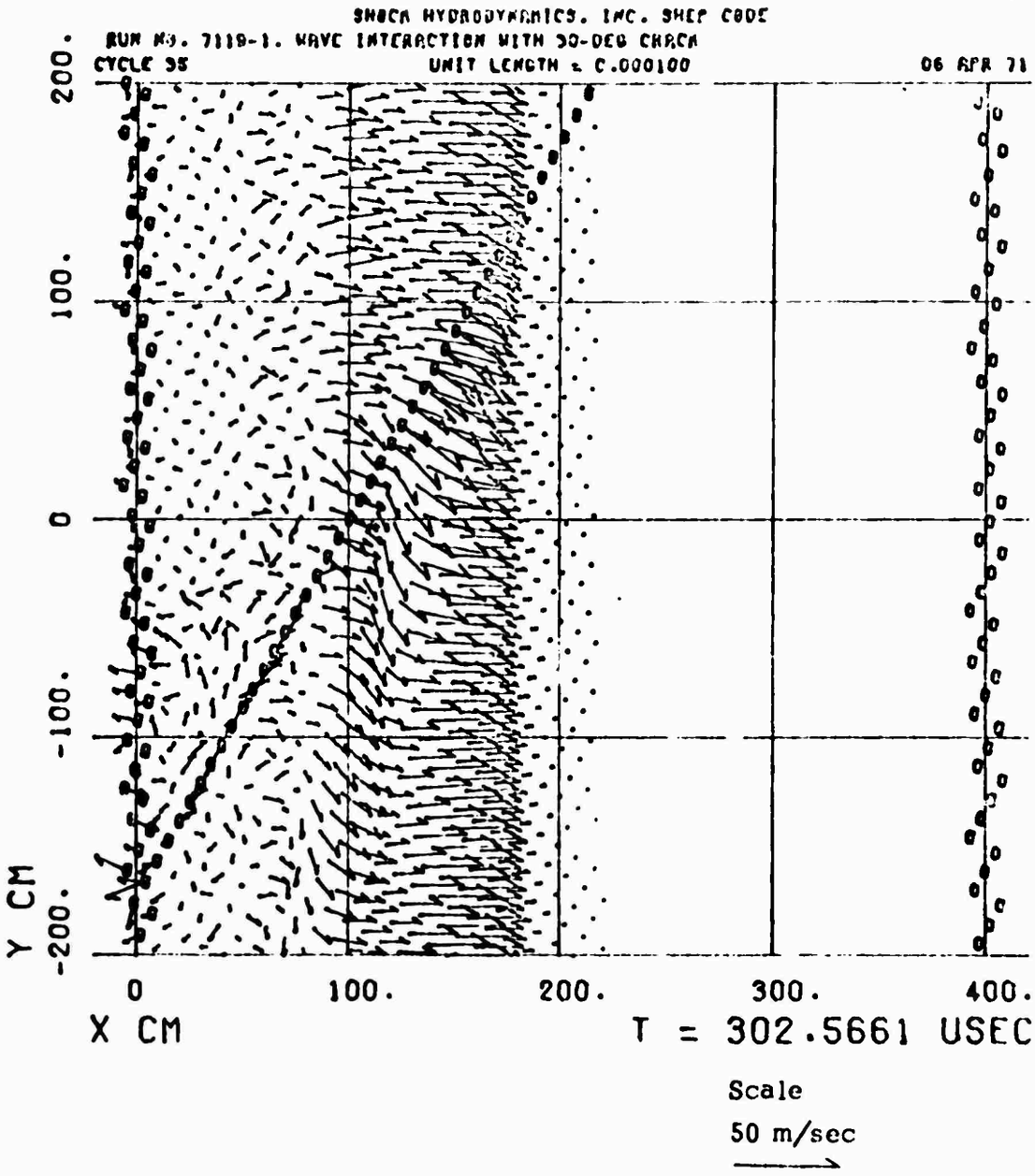

Figure 10. Particle Velocity Field, Case 1

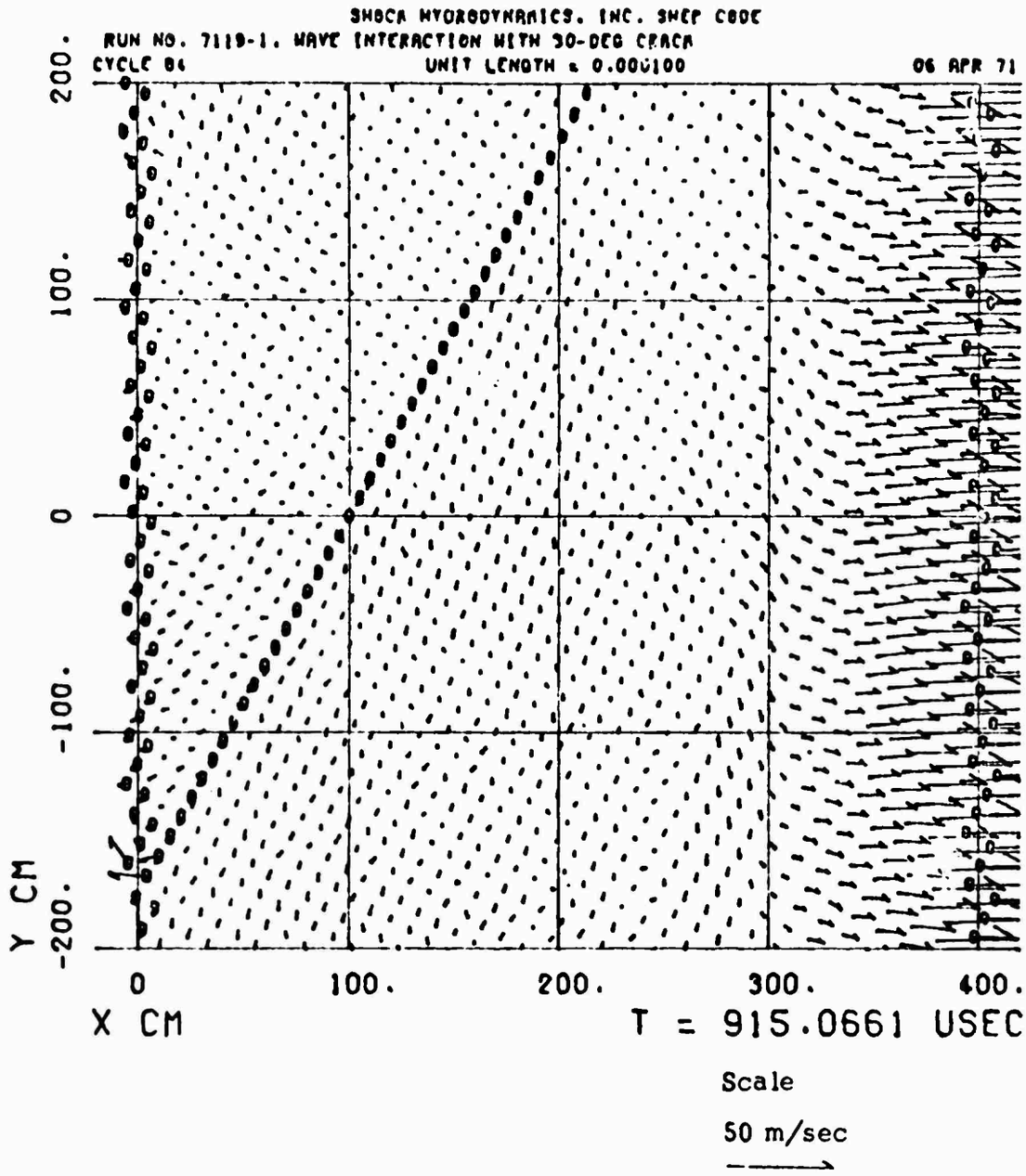

Figure 11. Particle Velocity Field, Case 1

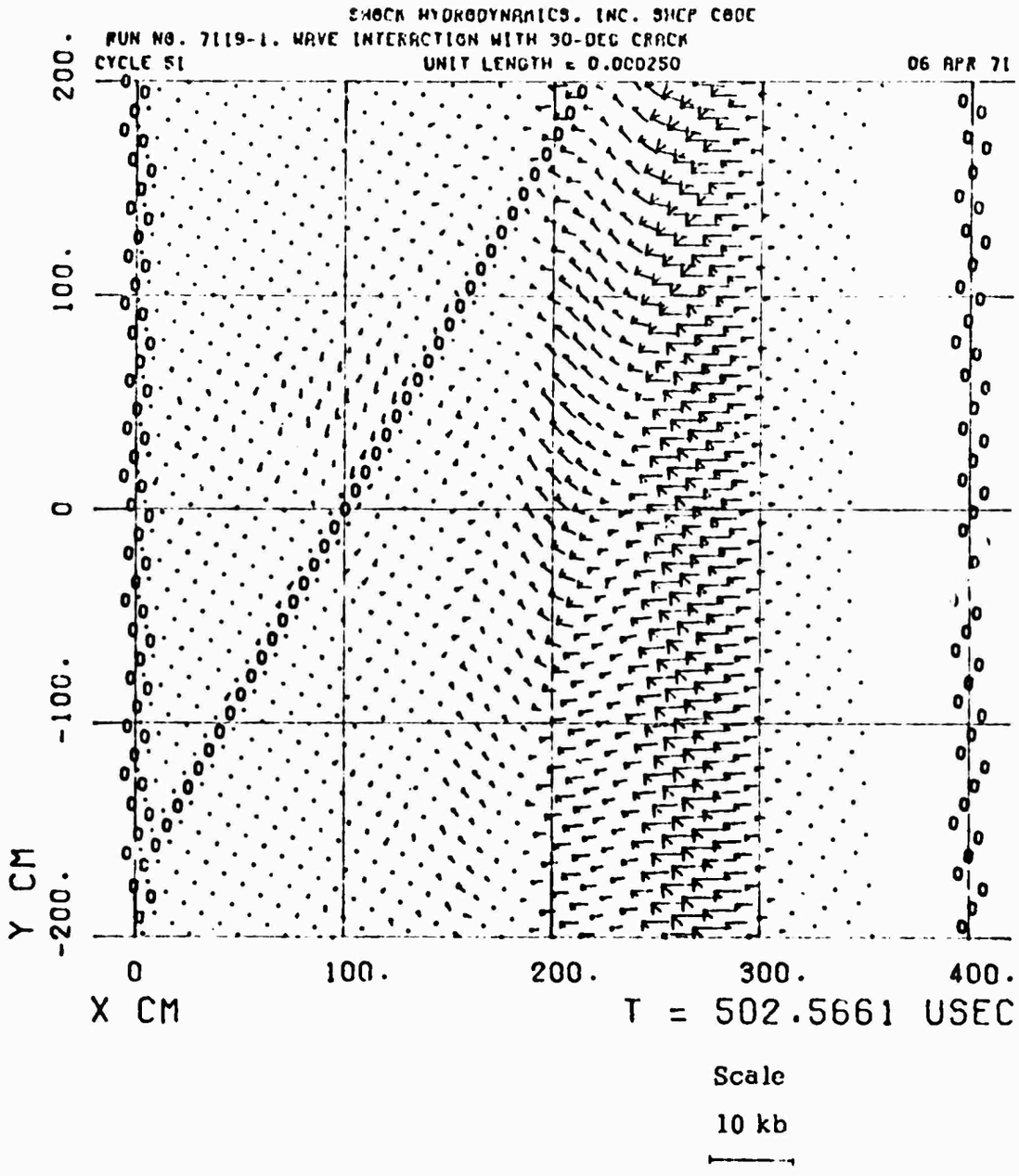

Figure 12. Principal Stress Field, Case 1

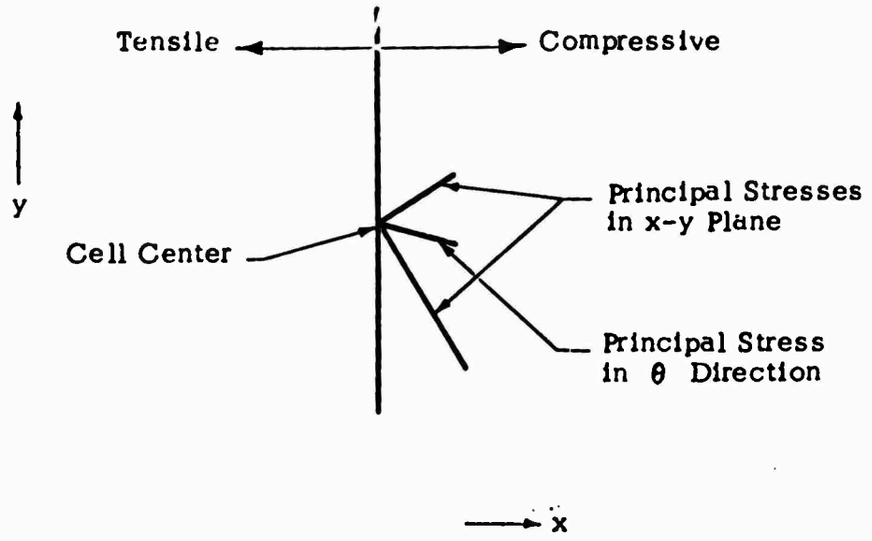

The edits of the velocity vector field plot the direction and magnitude of the velocity of each lattice point in the computing grid. The vector lengths for both the principal stress and velocity fields are scaled to the unit length indicated above each plot; the units are Mb/cm and (cm/μsec)/cm, respectively. On the more recently produced plots, the scale is also graphically depicted in the upper right hand corner.

As the stress wave interacts with the crack, the material on the right side of the crack is driven by the stress component normal to the crack, since shear stresses cannot be supported. As shown in Figure 10, the velocity vectors along the crack at the shock front are thus directed normal to the crack, turned downward 30°. Also, as shown in Figure 2, note that the principal stress tensors in the material along the right side of the crack are rotated into a direction transverse to the crack surface, again reflecting the fact that the crack surface can not bear shear stress. As the incident wave runs along the crack, a dilatational wave and trailing shear wave are formed which propagate across the block. The transmitted shock front remains approximately planar and oriented at 90° to the x axis. In the shear region behind the shock, a distinctly downward velocity flow is evident. This action induces material slippage along the crack, the material on the right side of

the crack moving downward and to the left, along the crack, relative to the material on the left side. In addition, there was a slight separation, or opening-up, of the materials on either side of the crack, which were initially in contact.

Time histories of the material displacement at the points indicated in Figure 13 were recorded during the code solution. The slippage of material initially at the point x = 100 cm, y = 0 cm, as given by the distance between points on opposite sides of the crack (points B and C in Figure 13), is shown in Figure 14. The extents of the downward (y-direction) displacements of these points are shown in the time histories given in Figure 15. The downward displacements of other points in the field, at x = 55, 158, 203, and 253 cm (points A, D, E, and F) along the central horizontal plane (y = 0), are shown in Figure 16. The forward (x-direction) displacements of these points during this time were all $\sim$ 0.25 cm. The perturbation of flow, as measured by the downward thrust of material, is seen to diminish as the distance from the crack increases.

Stress (σ_x) - time profiles at points A, D, E, and F are shown in Figure 17. The peak stress in the transmitted wave (points D, E, and F) is seen to be reduced by about 25% from that in the incident wave. The aforementioned two-wave structure in the transmitted wave and the reflected wave at point A are also displayed in these plots.

3.4 CASE 2 - INTERACTION OF STRESS WAVE WITH SINGLE, FINITE-LENGTH CRACK

The initial configuration of the Lagrangian grid set up for this problem is shown in Figure 18. The crack extends from the loading surface (lower left) to the crack tip at x = 200 cm, y = 0.

Representative results of the SHEP code solution of this problem, as depicted by the particle velocity fields for times of .3, .4, .5, .6, and 1 msec, are shown in Figures 19 to 22 and in Figure 4 in the Summary, Section 2.3.1. Associated principal stress fields for times of .4, .5, and

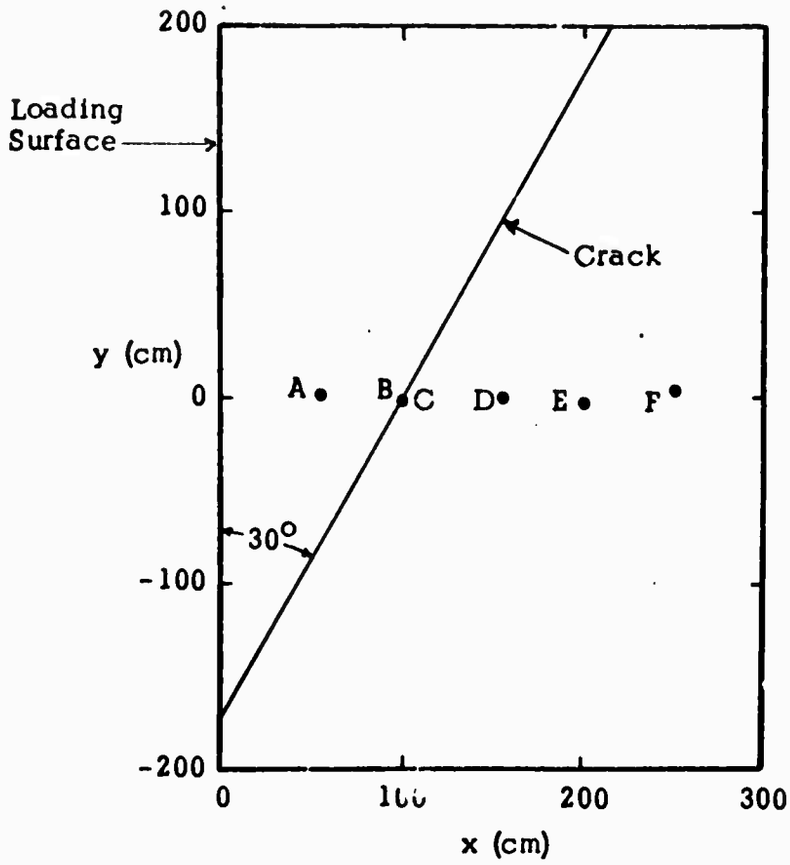

Figure 13. Location of Time History Data Stations

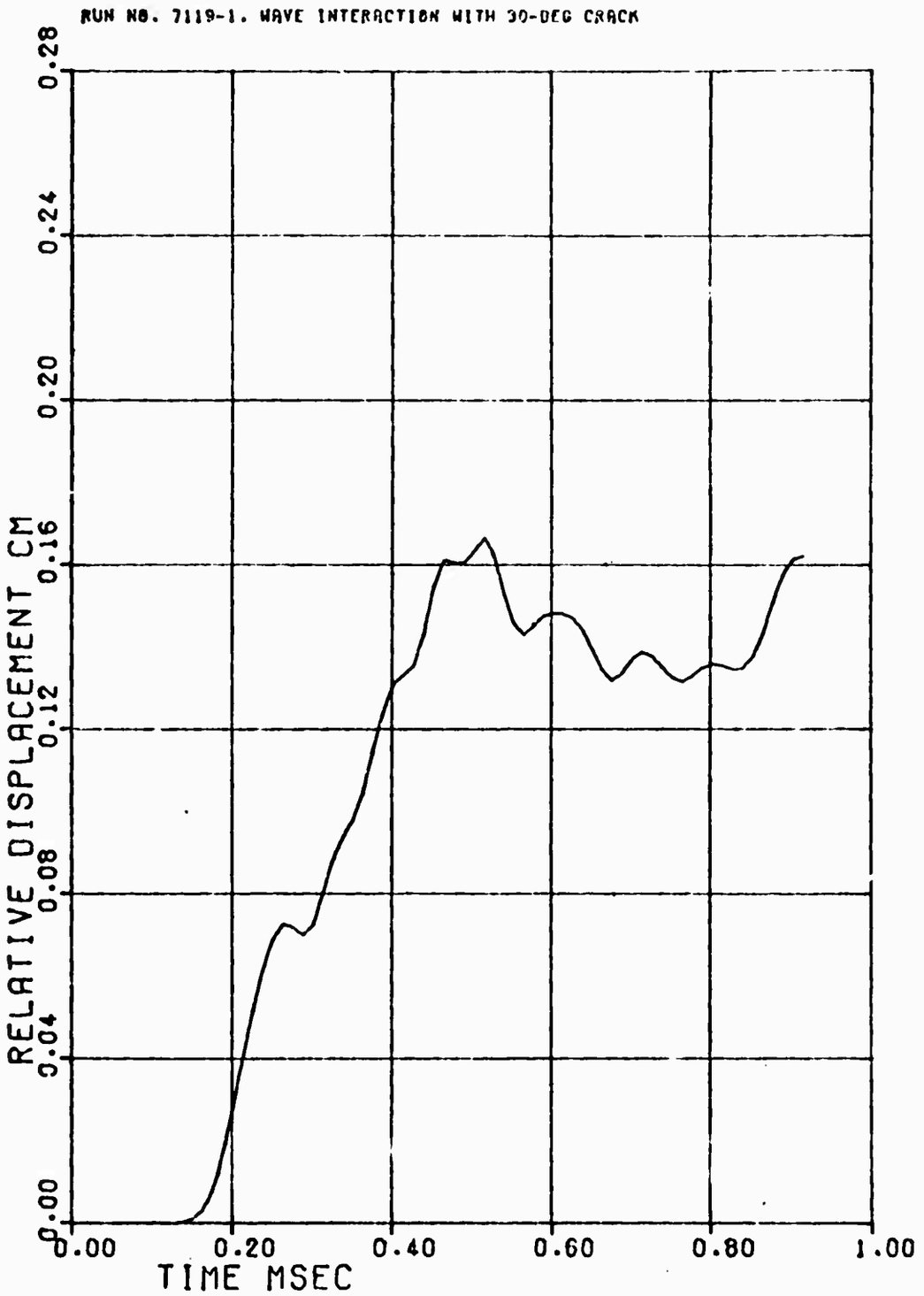

Figure 14. Material Slippage Along Crack at x = 100 cm, y = 0, Case 1

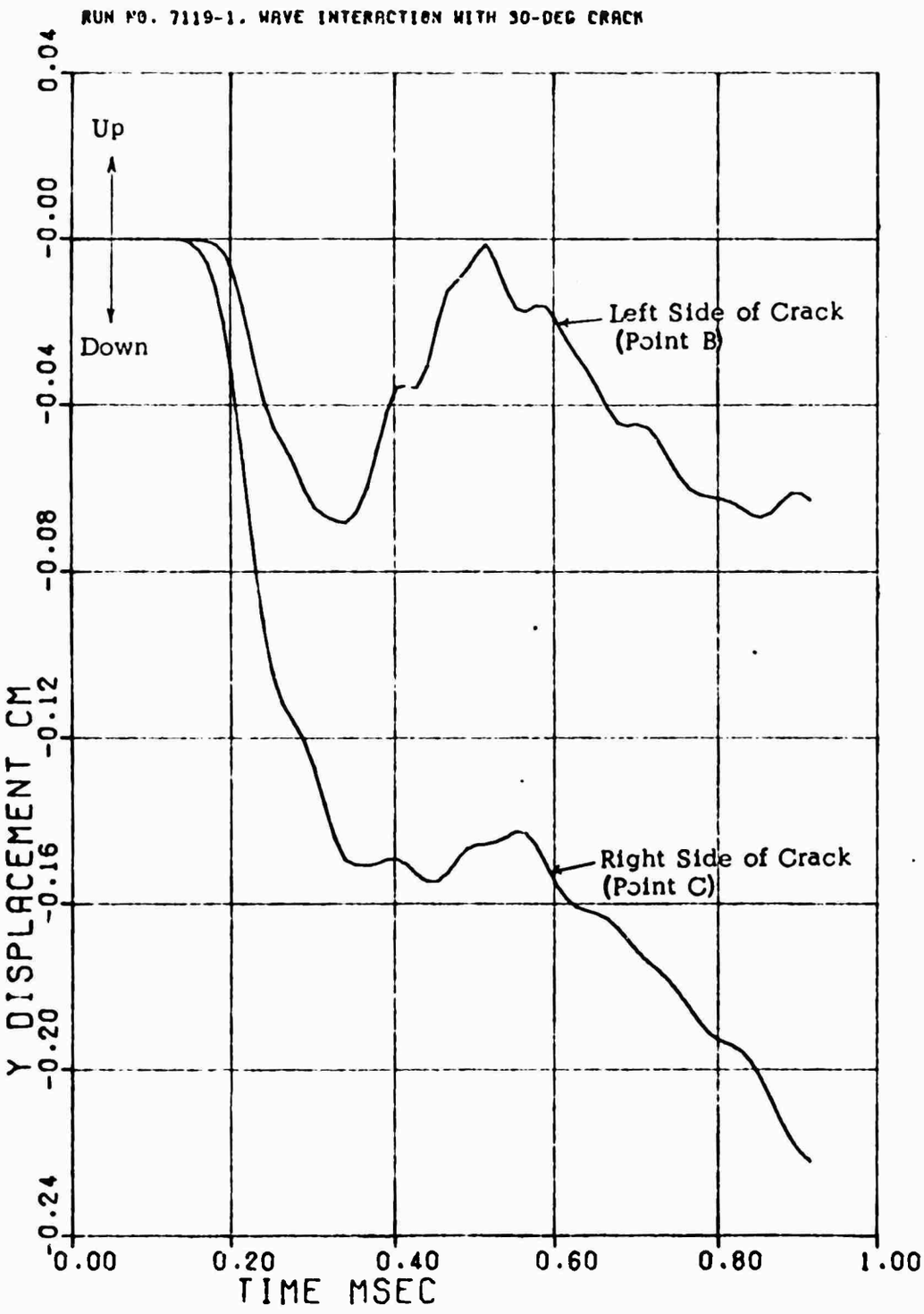

Figure 15 Vertical Displacement of Material Along Crack at $x = 100$ cm, $y = 0$, Case 1.

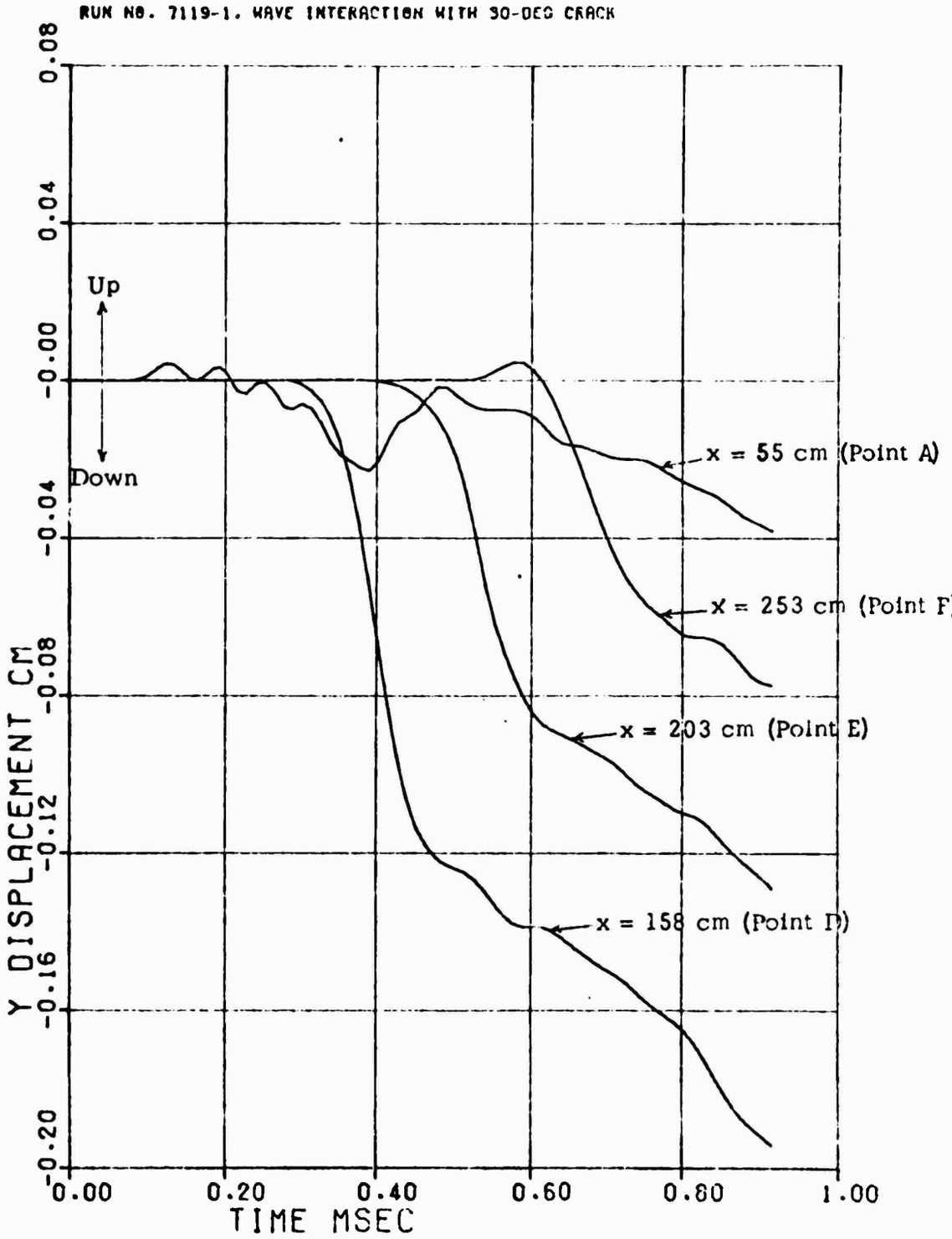

Figure 16. Vertical Displacement at Four Stations Along the y = 0 Plane, Case 1.

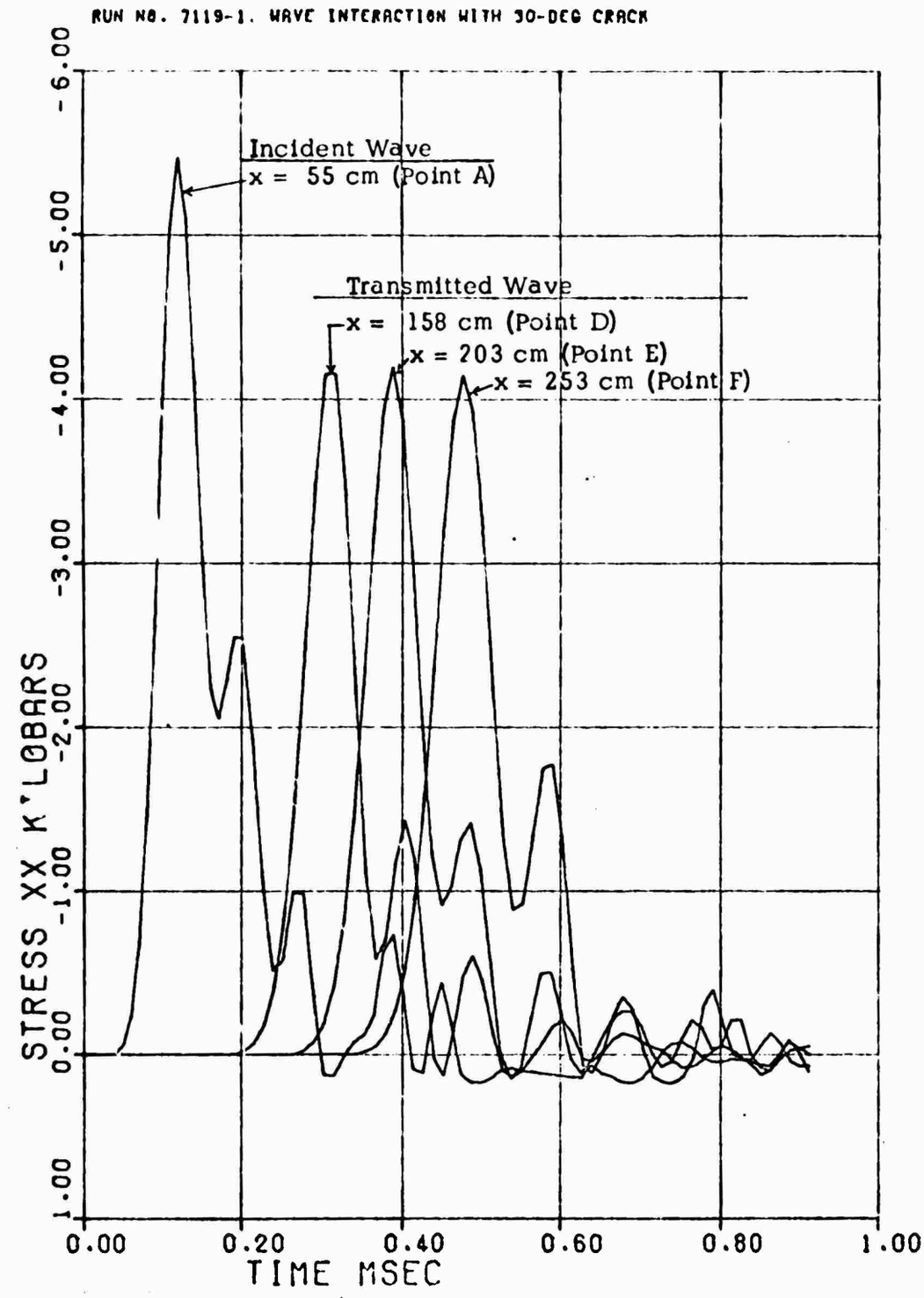

Figure 17. Stress (σ_x) Profiles at Four Stations Along the y = 0 Plane, Case 1.

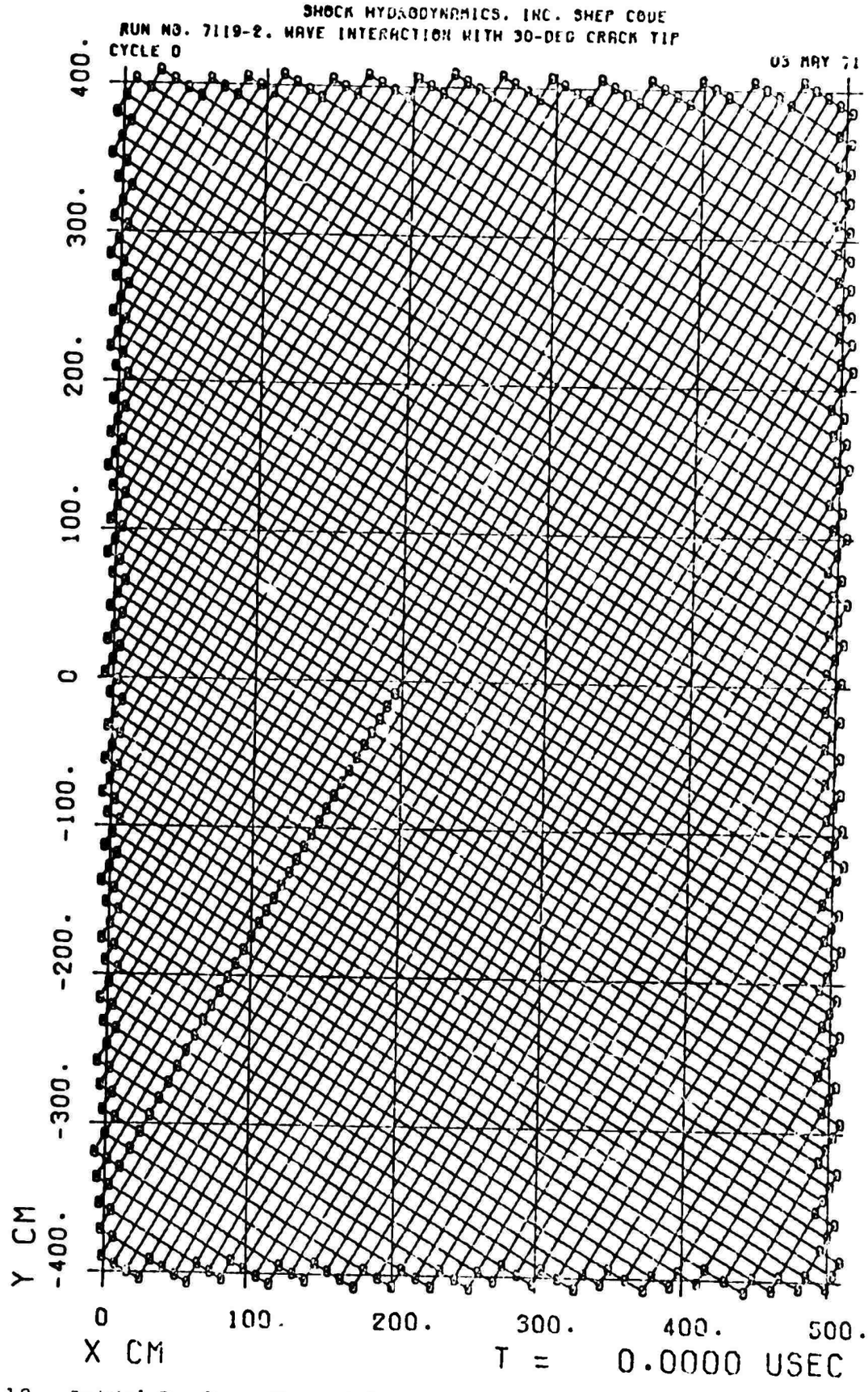

Figure 18. Initial Configuration of the Lagrangian Computational Grid, Case 2

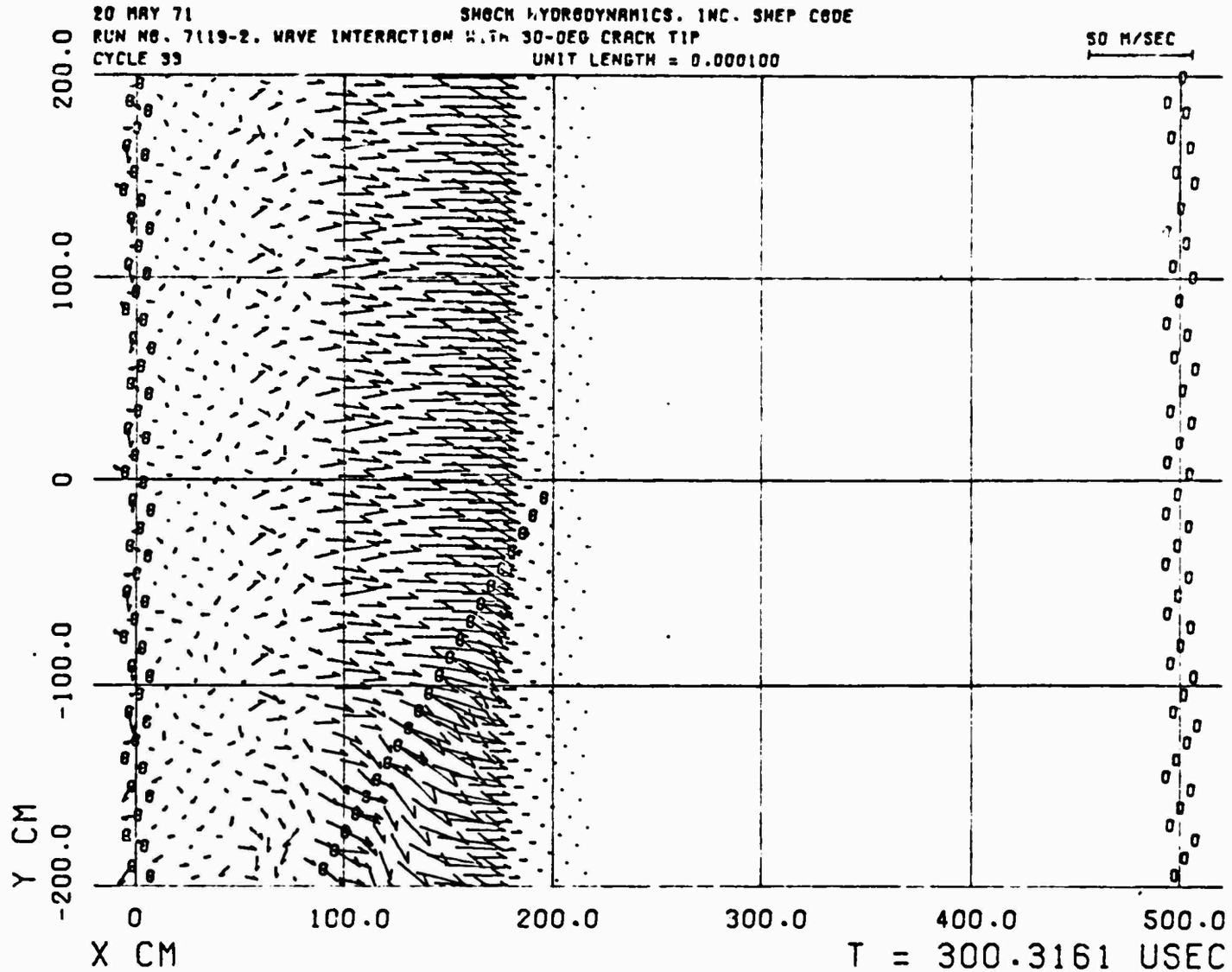

Figure 19. Particle Velocity Field, Case 2.

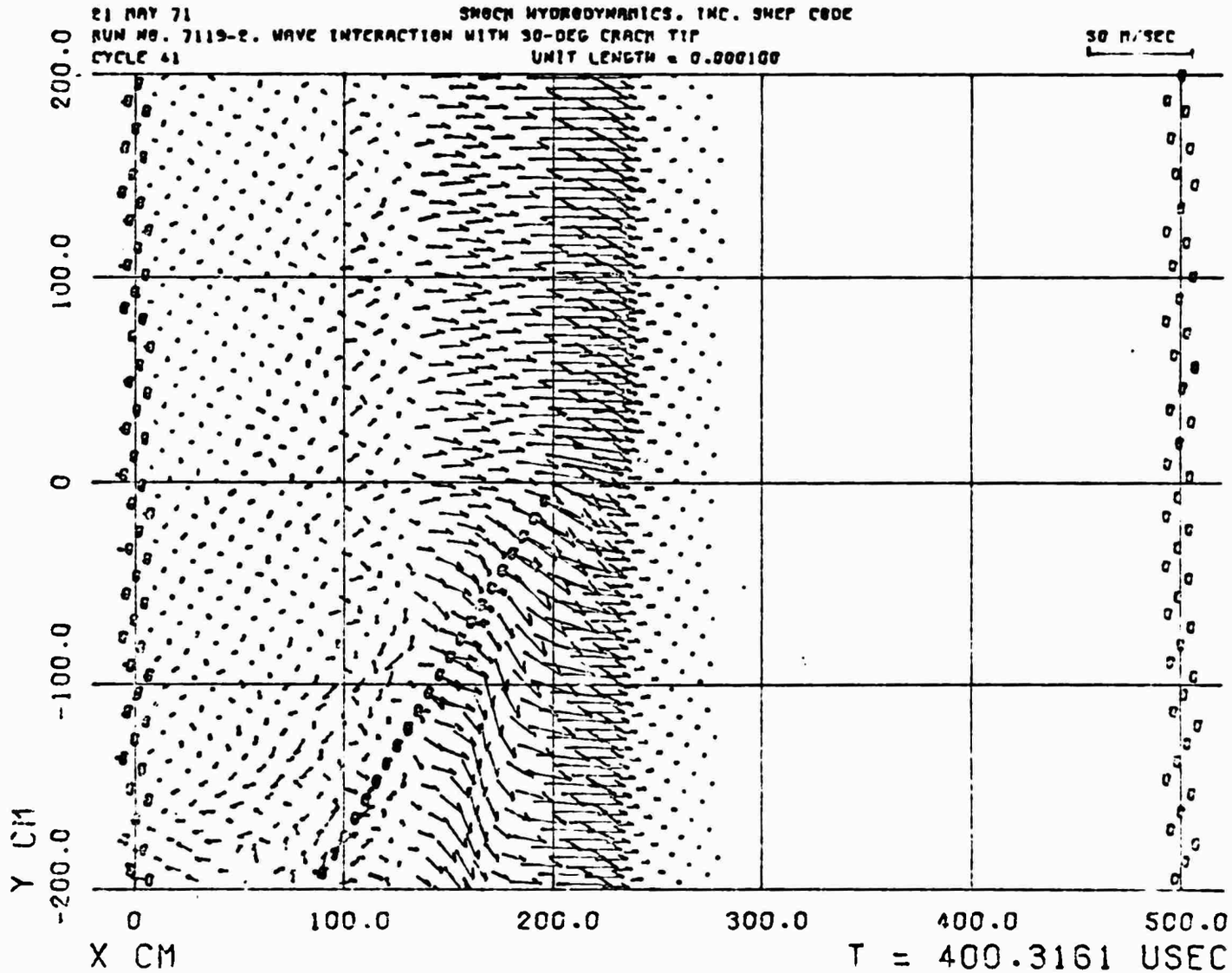

Figure 20. Particle Velocity Field, Case 2.

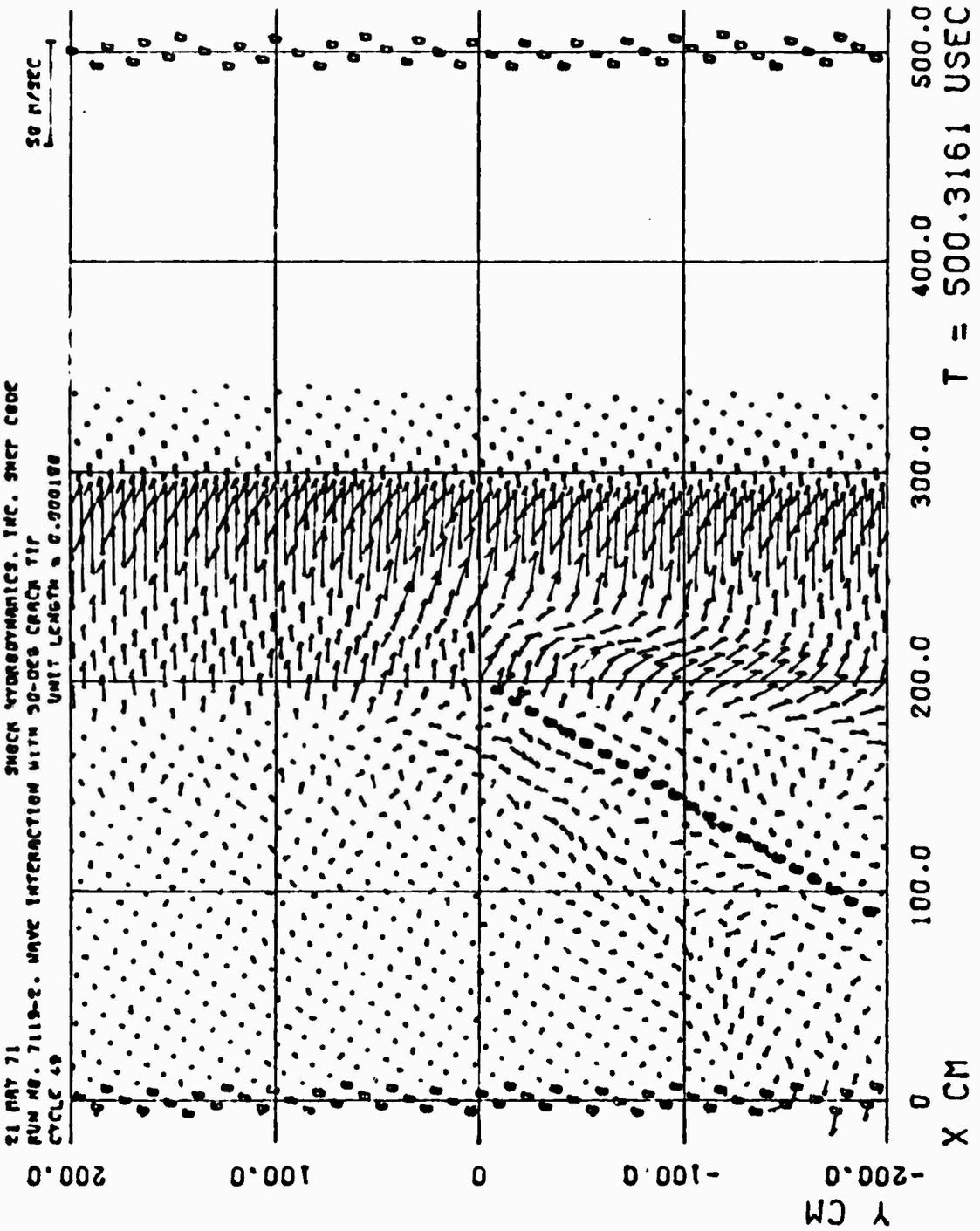

Figure 21. Particle Velocity Field, Case 2

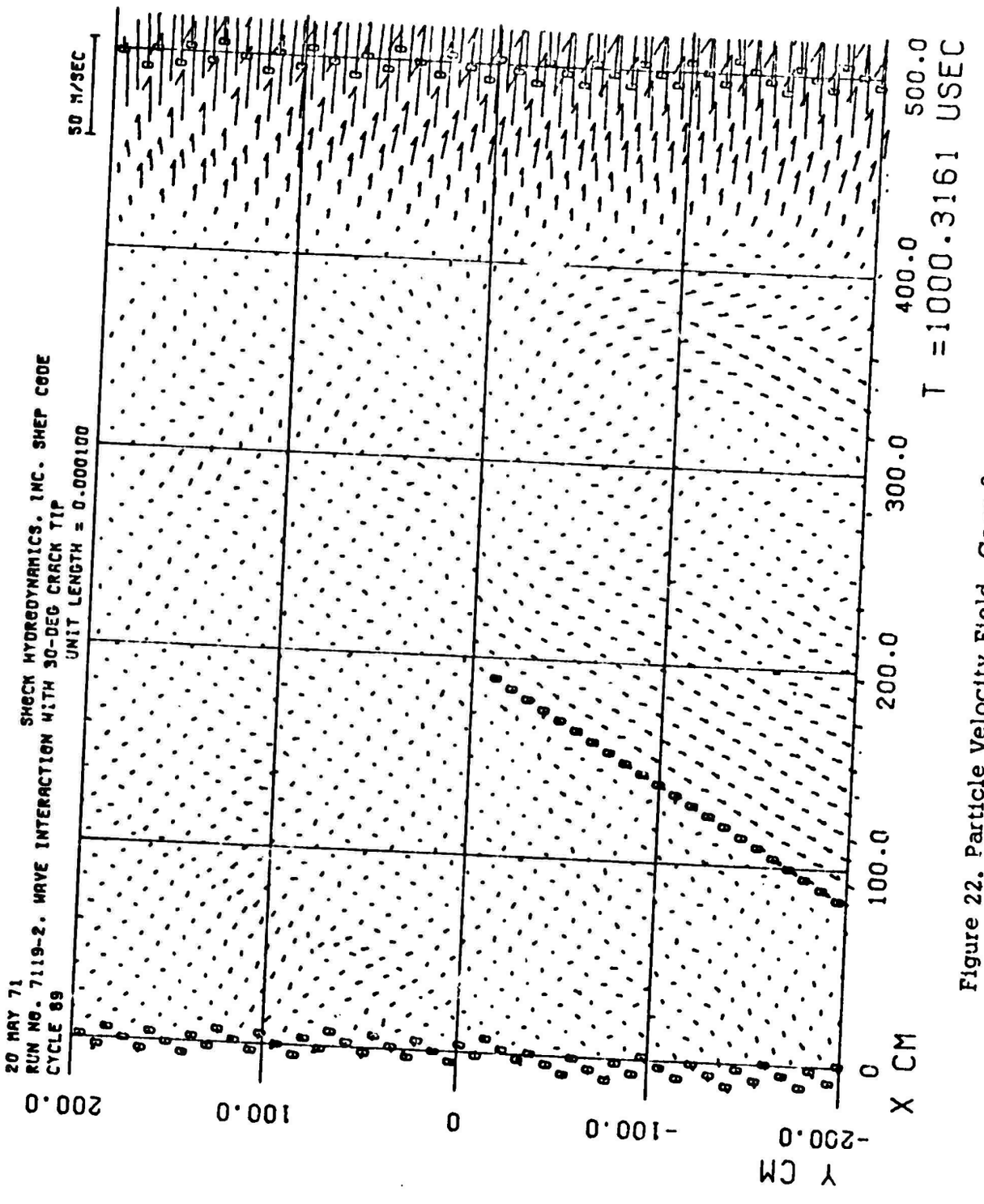

Figure 22. Particle Velocity Field, Case 2.

.7 msec are shown in Figures 23 to 25. For clarity in reading these plots, the field of view is limited to the central region of interest.

The response of the granite in this problem is, of necessity, similar to that in the infinite-crack problem, until the wave front reaches the crack tip. Subsequently, the wave system is divided approximately in half, the part above the crack tip appearing as a simple plane wave, and that below as a dilational wave and trailing shear wave, as in the previous solution. Starting from the crack tip, a disturbance, or bow wave, propagates into the plane wave region above and the "cracked" region below, altering both flow fields and creating an expanding region of transition between them. The diversion of flow around the crack tip may be seen in Figures 19 and 20.

Time histories of the material displacement at the locations indicated in Figure 26 were recorded during the code solution. The slippage of material at three points along the crack, as given by the distance between points on opposite sides of the crack, designated as (W,X), (R,S), and (M, N) in Figure 26, is shown in Figure 27. The material on the right side of the crack is moving downward and to the left, along the crack, relative to the material on the left side. The extents of the downward (y-direction) displacements of these points and the crack tip (point I) as a function of time are shown in Figure 28. The spatial trajectory of the point pair (W,X) on the crack surface during the time span of the solution is plotted in Figure 29. Time-histories of the vertical displacements of points above and below the crack tip along four vertical cuts ($x \approx$ constant) through the target are shown in Figures 30 to 33. The downward shift of material persists at all these stations, but in smaller amounts as the distance from the crack increases.

Stress (σ_x) - time profiles at points H, I, J, and K, along the horizontal plane through the crack tip ($y \approx 0$), are shown in Figure 34. Note the increase in stress over that of the loading level near the crack tip. Stress profiles along the vertical plane through the crack tip ($x \approx 200$ cm) are shown in Figure 35. The points above the crack tip show a peak stress of 5 kb - corresponding to the loading or incident shock level, and those below the tip to about 4 kb - the transmitted stress level. Stress-time profiles along a vertical plane to the right of the crack tip, at $x \approx 300$ cm, are shown in

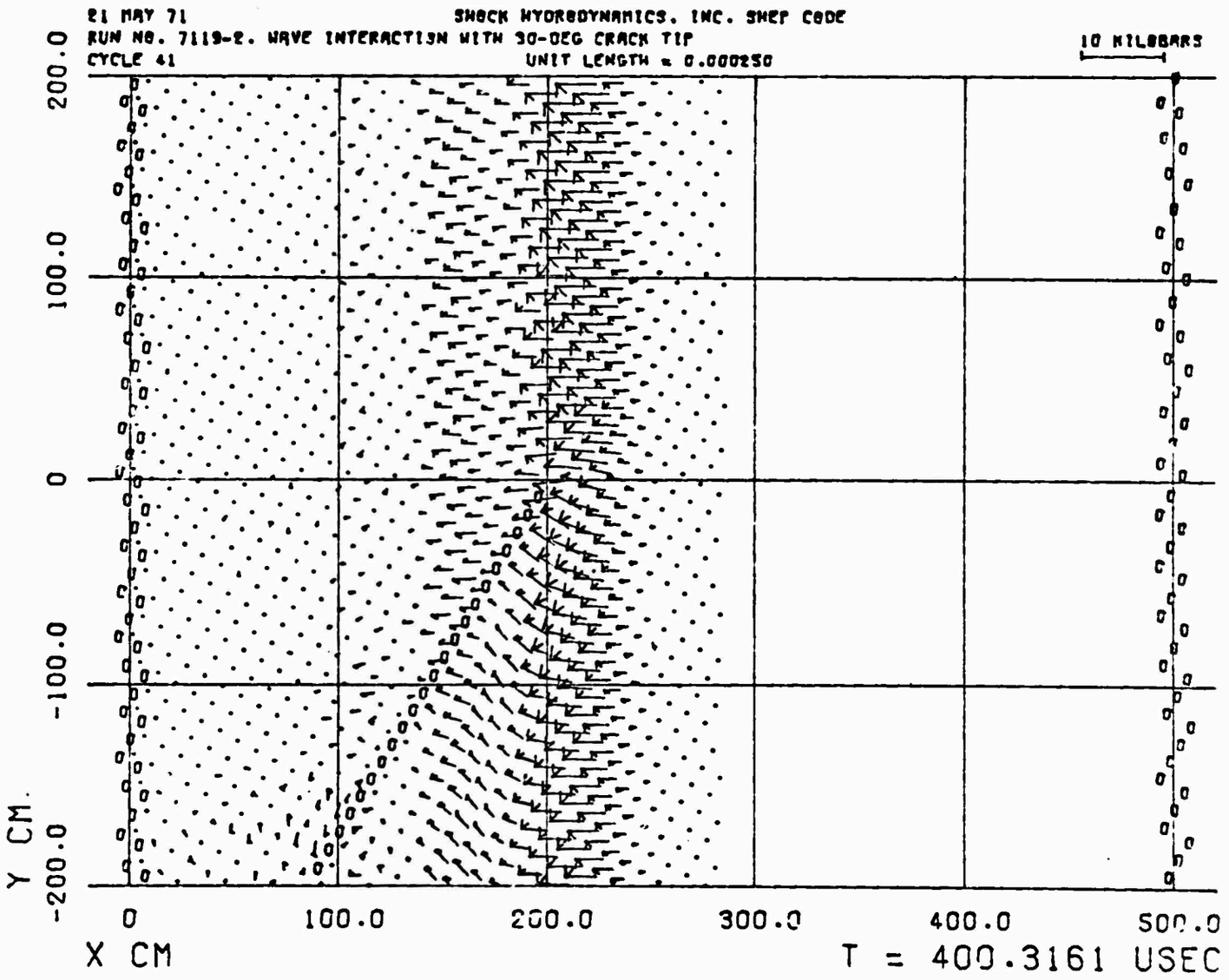

Figure 23. Principal Stress Field, Case 2.

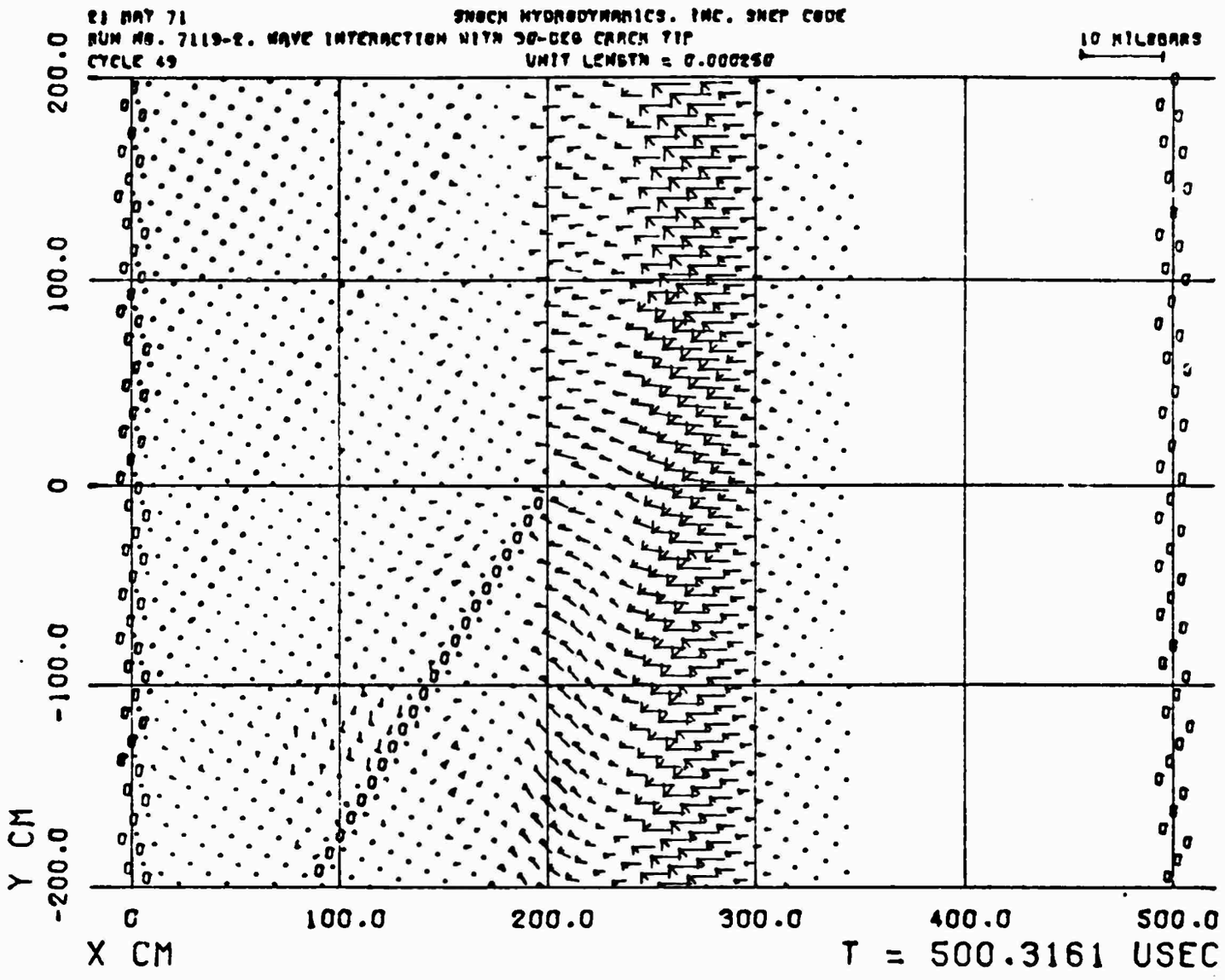

Figure 24. Principal Stress Field, Case 2.

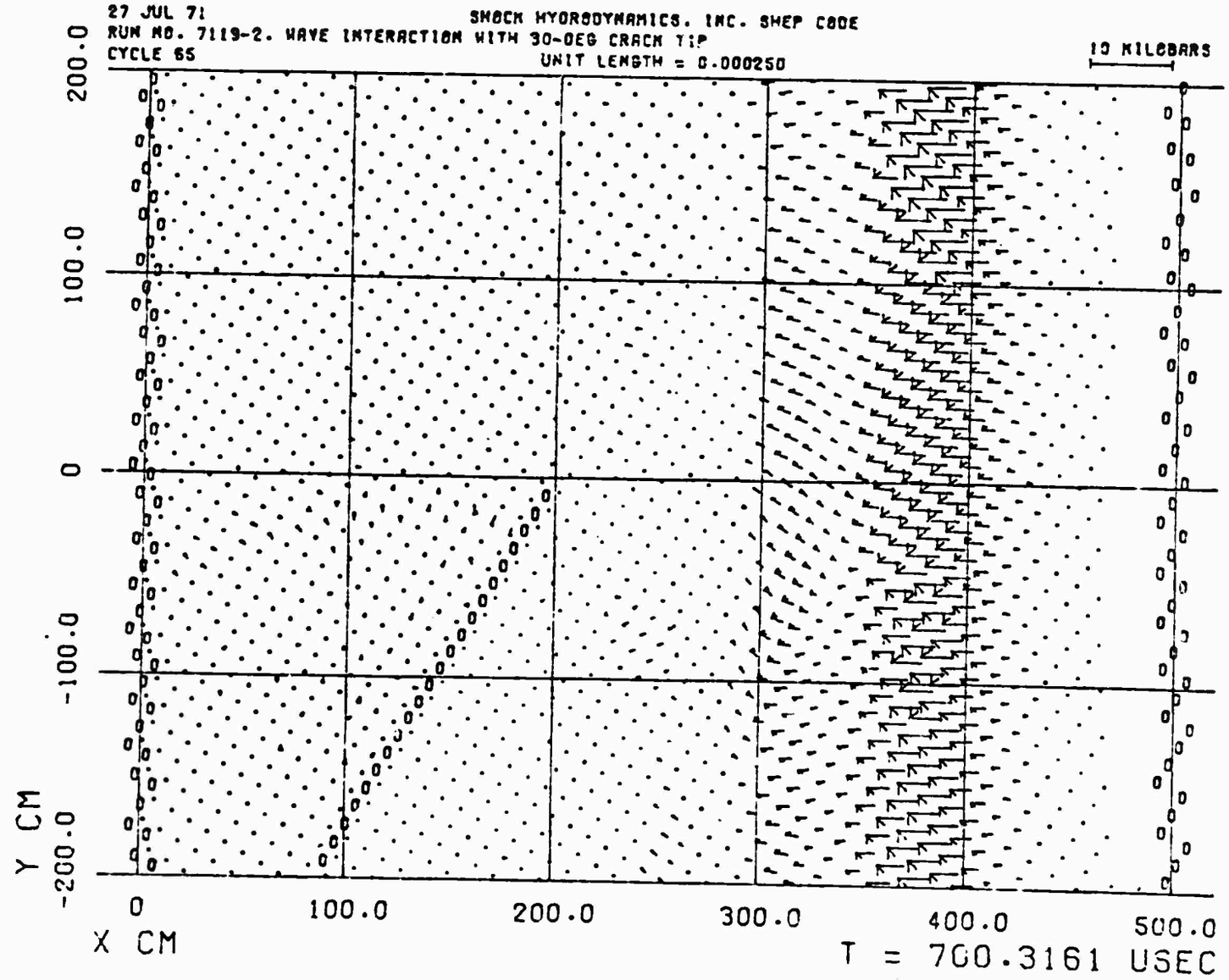

Figure 25. Principal Stress Field, Case 2.

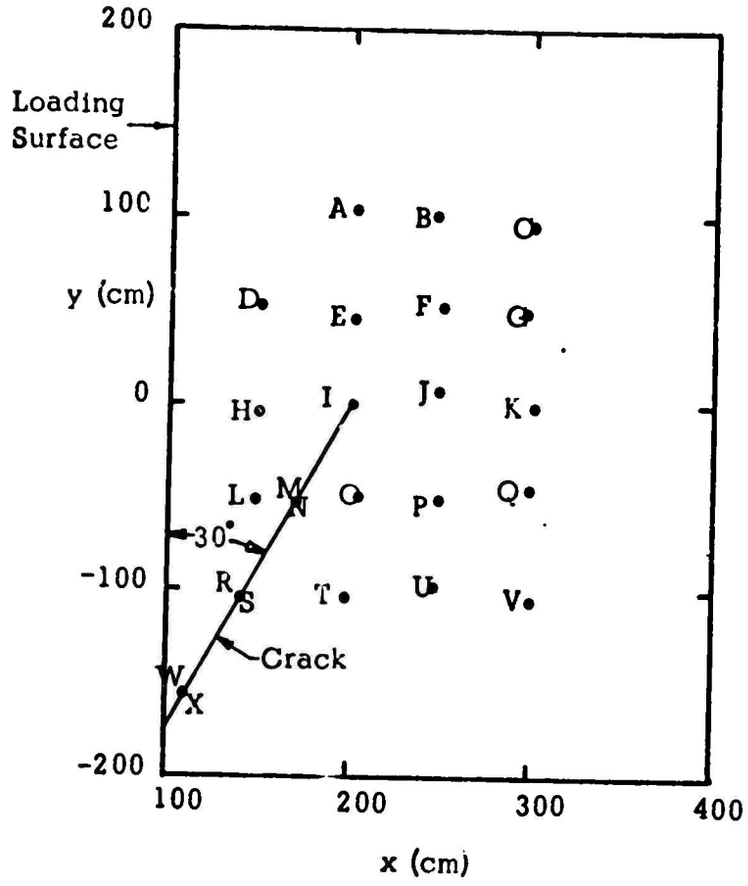

Figure 26. Locations of Time History Data Stations, Case 2.

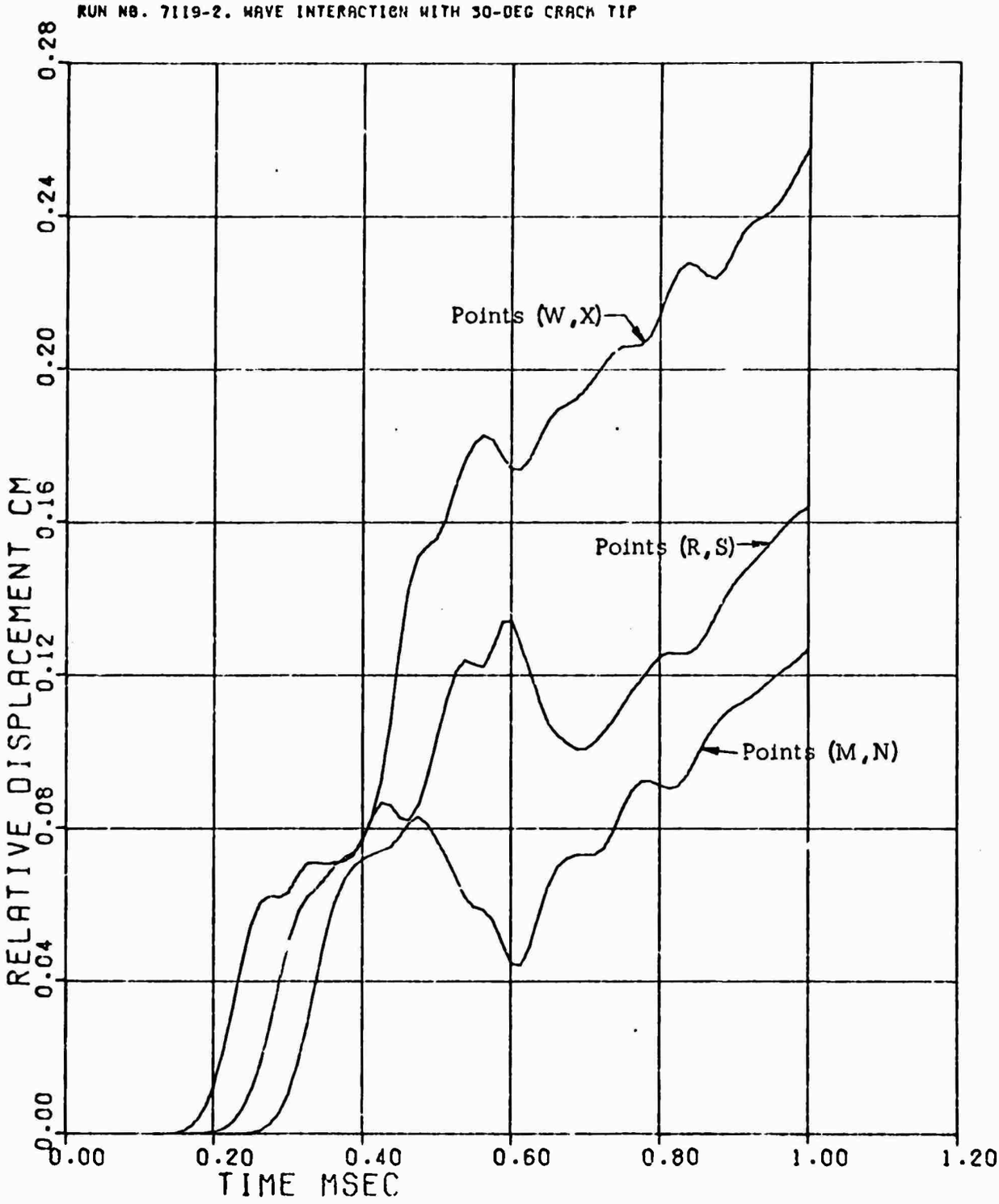

Figure 27. Material Slippage at Three Points Along the Crack, Case 2.

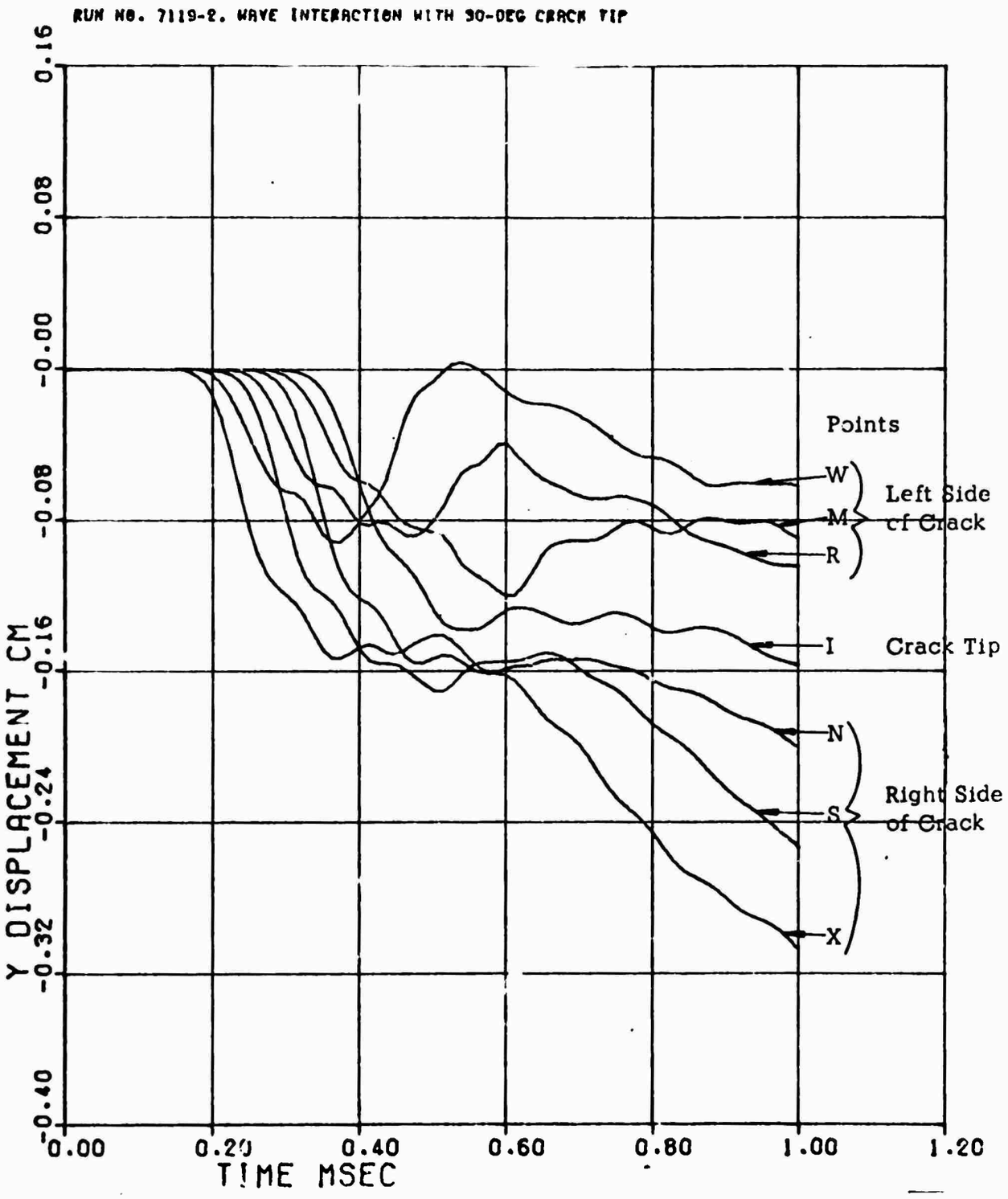

Figure 28. Vertical Displacement at Several Points Along the Crack, Case 2.

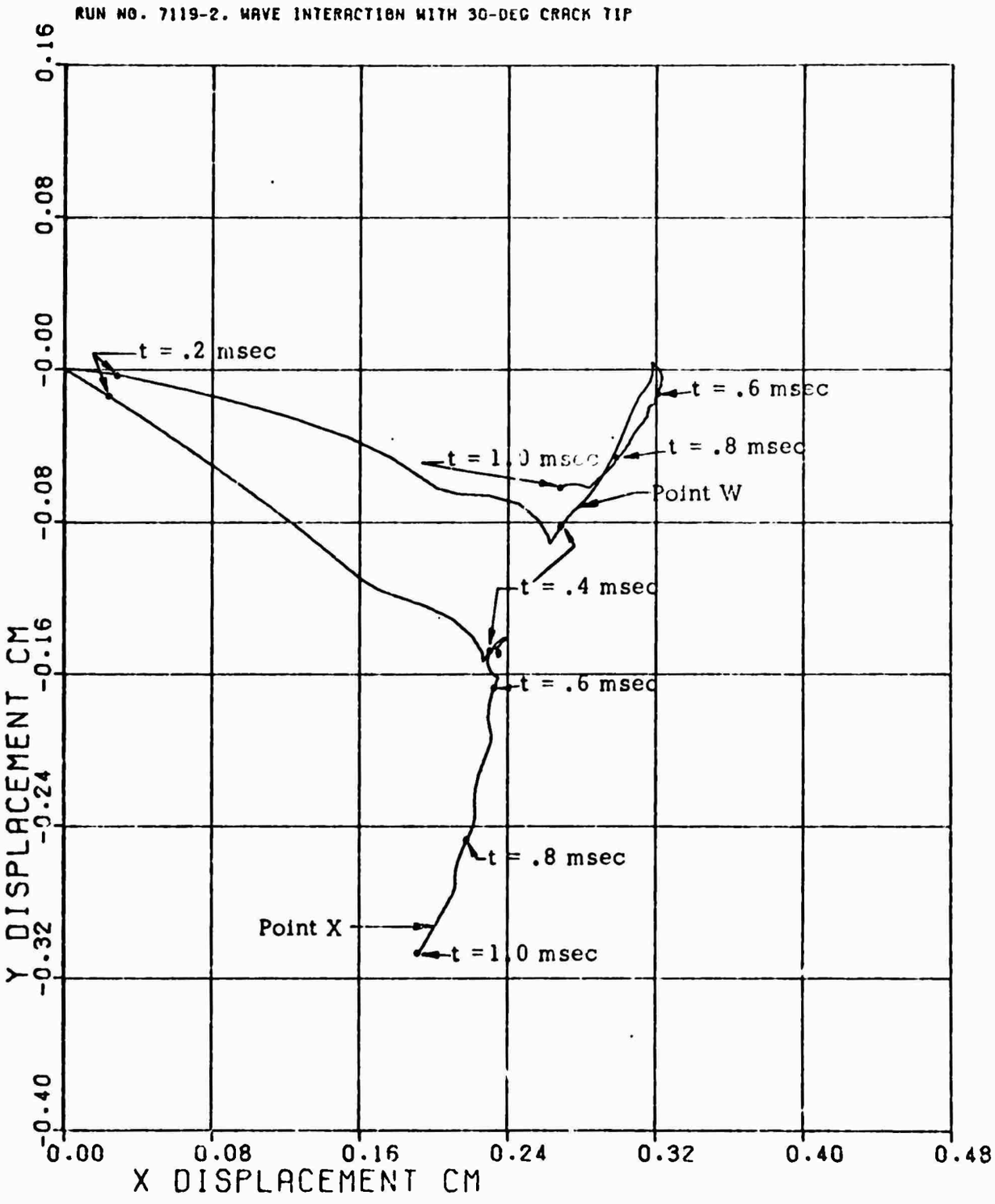

Figure 29. Spatial Trajectory of Two Initially Opposite Points on the Crack Surface, Case 2.

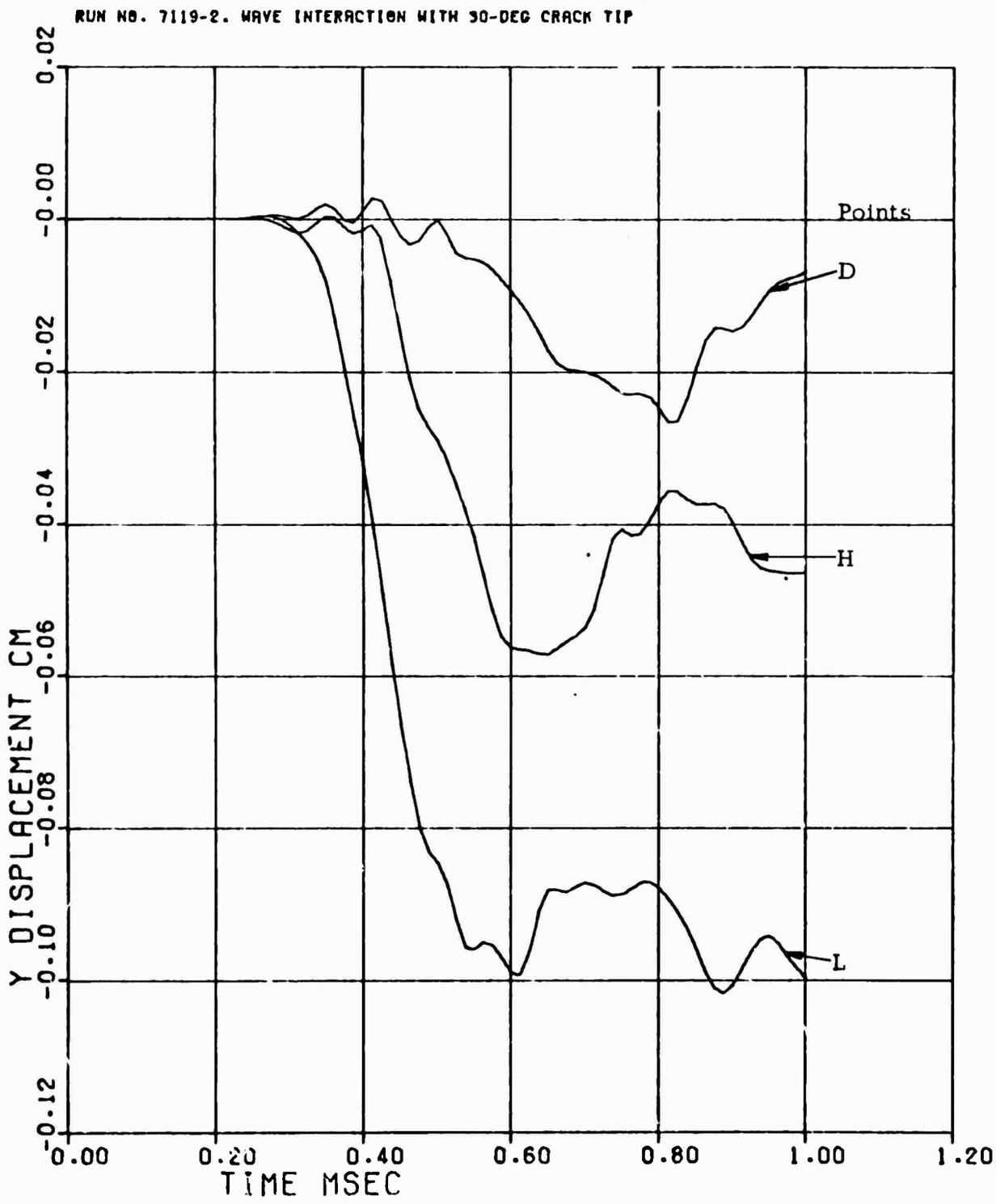

Figure 30. Vertical Displacement at Points Along the Vertical Plane at $x \approx 150$ cm, Case 2.

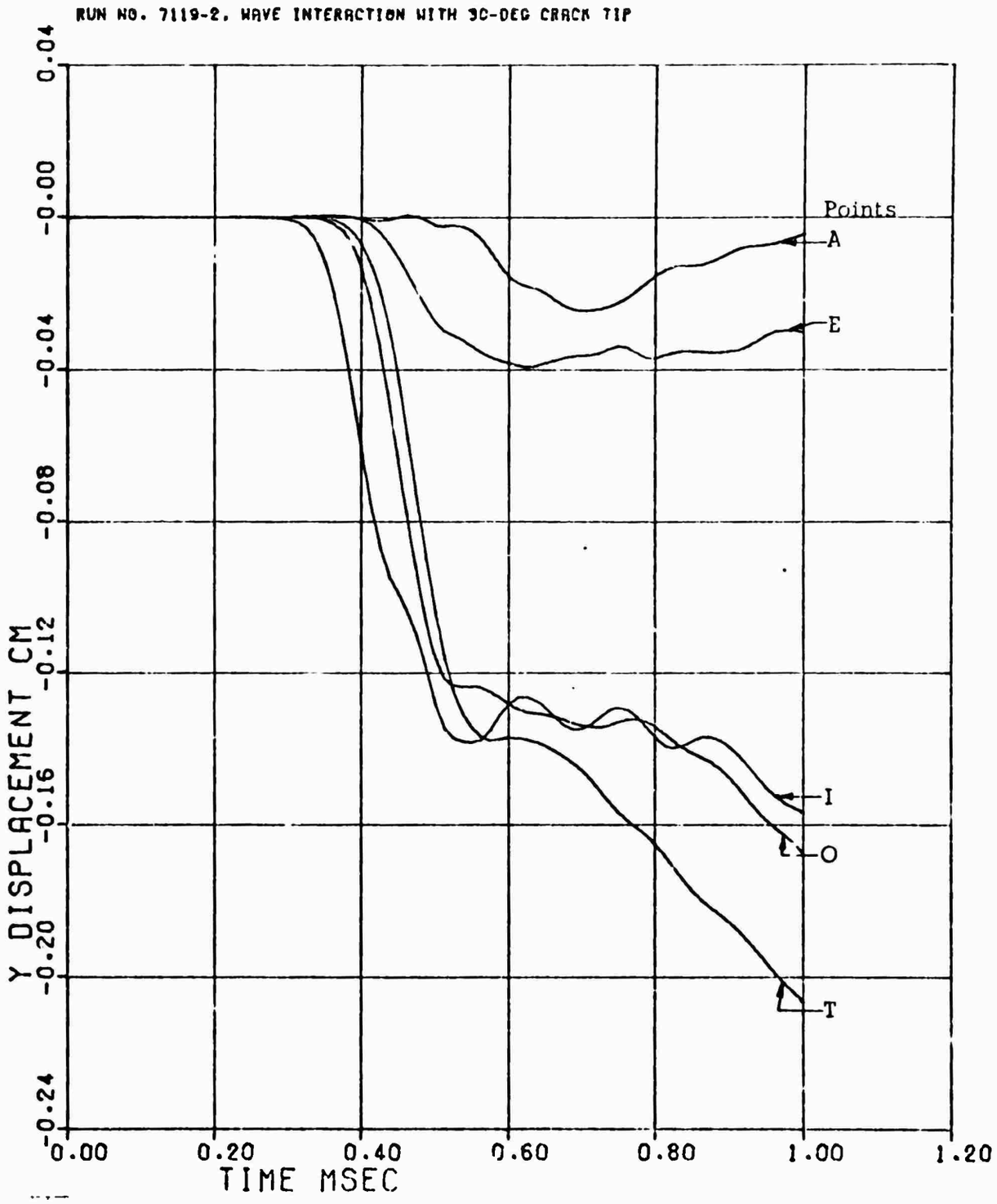

Figure 31. Vertical Displacement at Points Along the Vertical Plane at x ≈200 cm, Case 2.

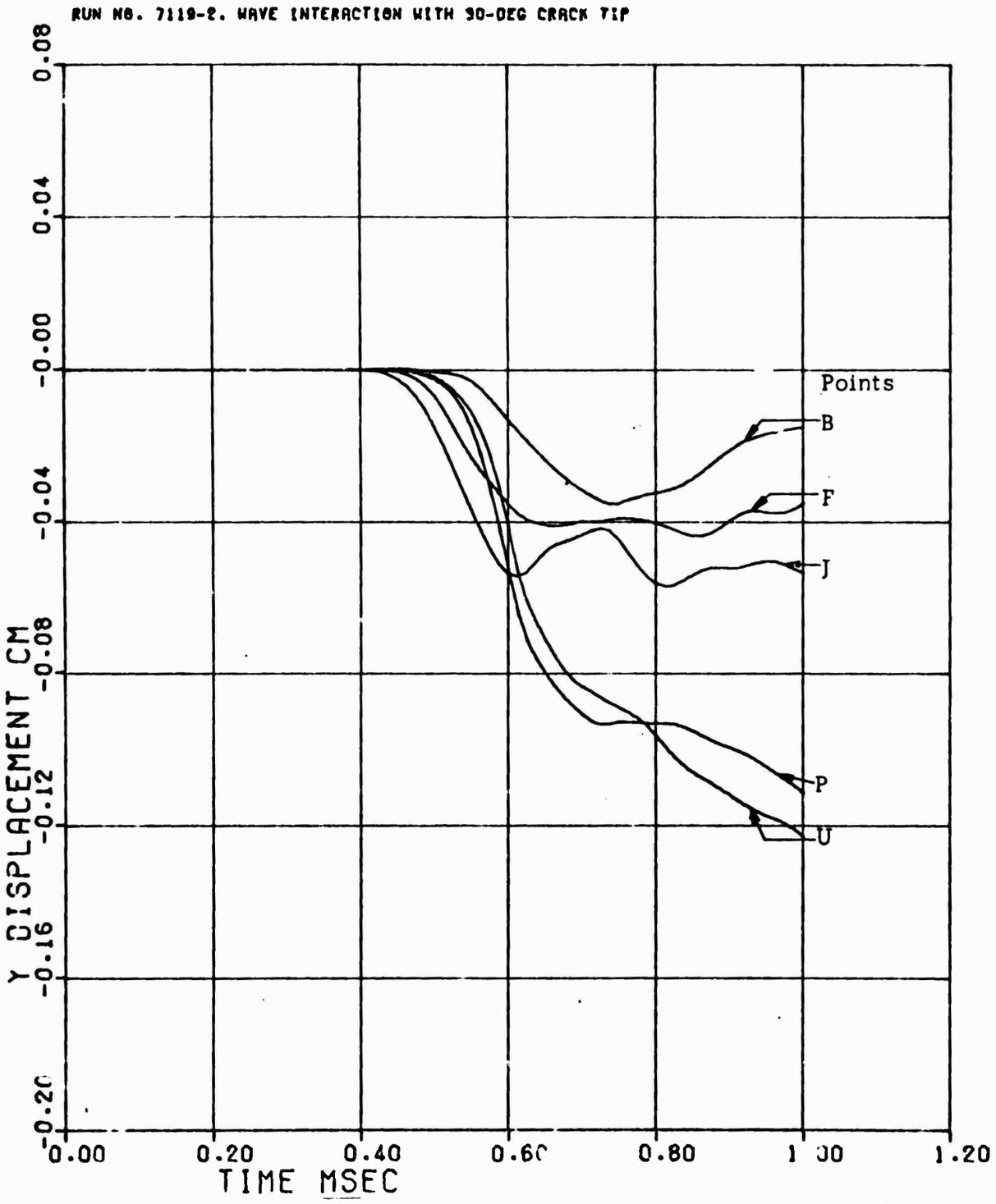

Figure 32. Vertical Displacement at Points Along the Vertical Plane at x ≈ 250 cm, Case 2.

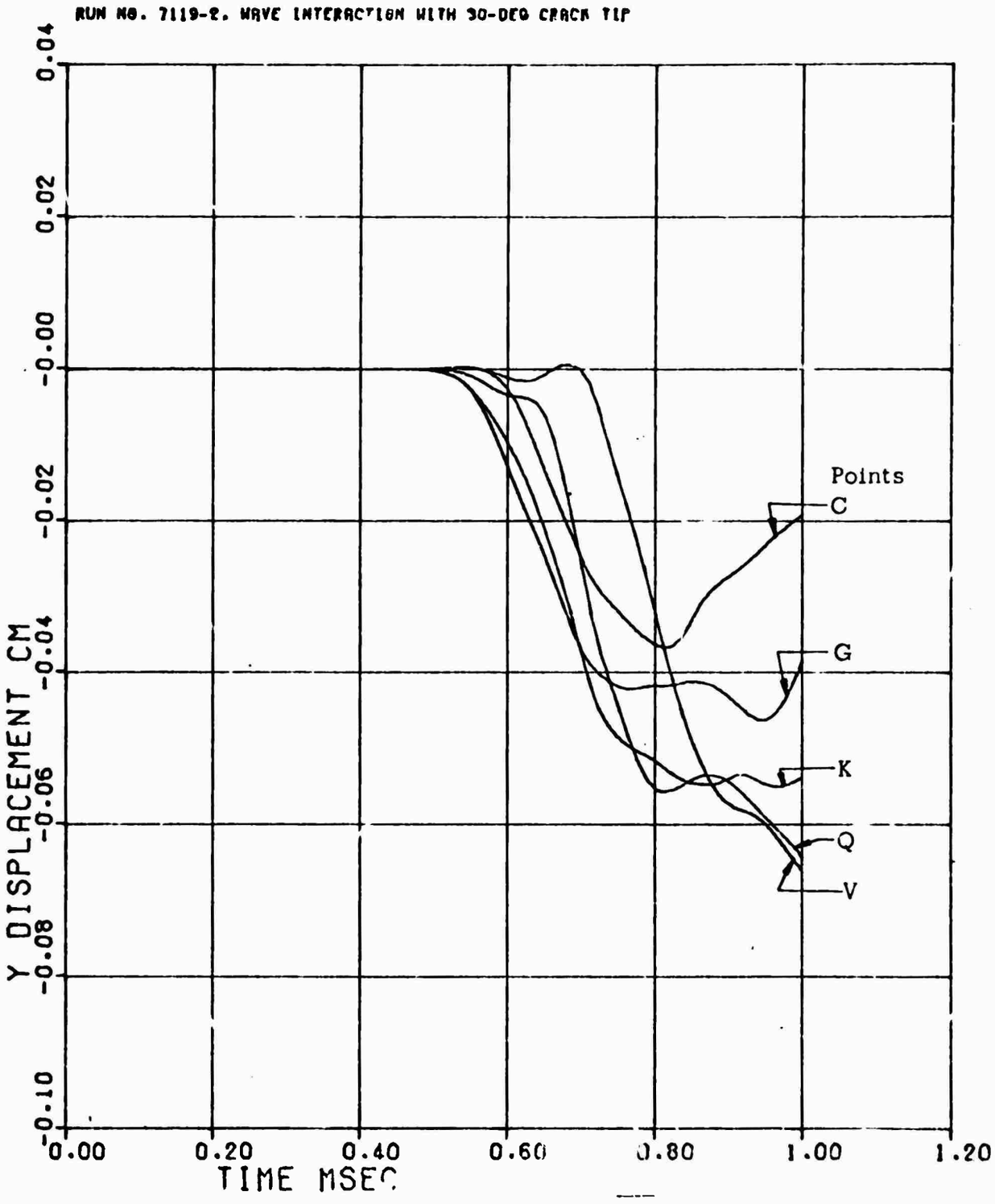

Figure 33. Vertical Displacement at Points Along the Vertical Plane at x ≈ 300 cm, Case 2.

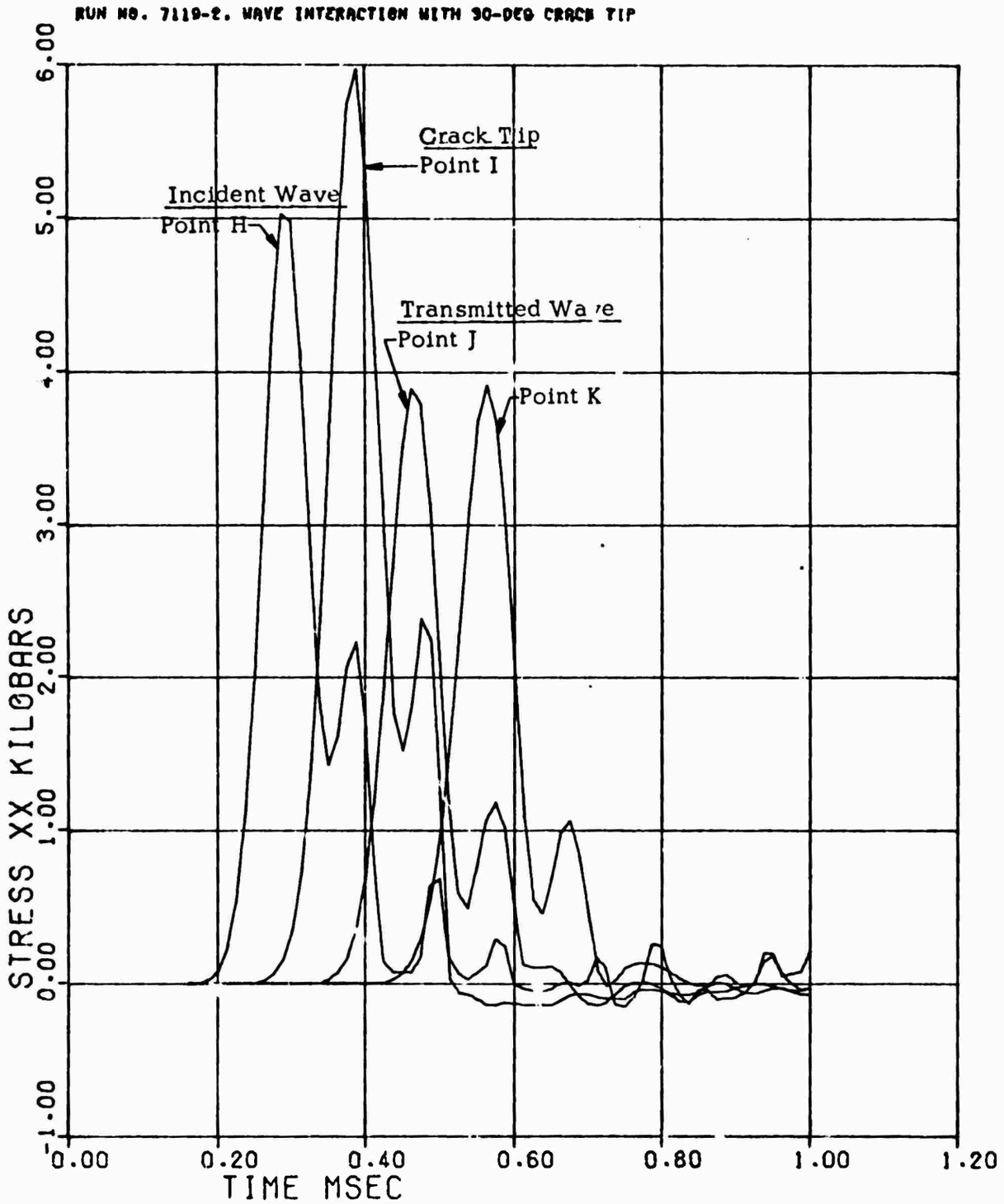

Figure 34. Stress (σ_x) Profiles at Points Along the Horizontal Plane at $y \approx 0$, Case 2.

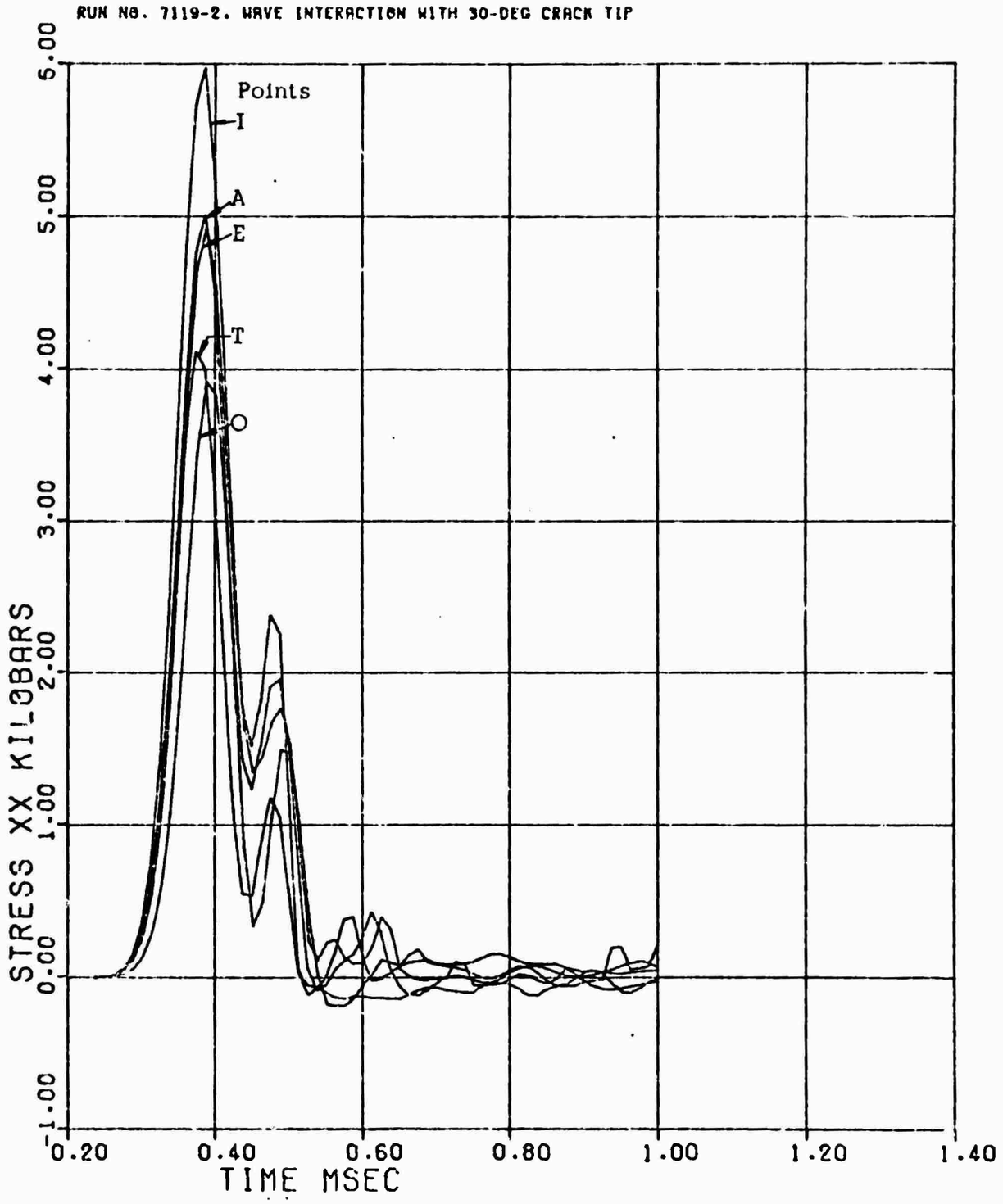

Figure 35. Stress (σ_x) Profiles at Points Along the Vertical Plane at $x \approx 200$ cm, Case 2.

Figure 36. Here the stress level is reduced at points above as well as below the crack tip. Time histories of the shear stress (σ_{xy}) at points along the vertical plane through the crack tip are shown in Figure 37.

3.5 CASE 3 - INTERACTION OF STRESS WAVE WITH SINGLE, FINITE-LENGTH CRACK, WITH CRACK GROWTH

For this case, the same problem as in Case 2 was solved, but with the provision in the code for permitting growth of the crack activated, as described previously.

Representative results of this code solution, as shown by the particle velocity fields for times of .5, .6, .7, and .9 msec, are given in Figures 5 to 7 in the Summary, Section 2.3.1, and in Figure 38. Associated principal stress fields for times of .5 and .6 msec are shown in Figures 39 and 40. Propagation of the crack does occur for this loading; the extent of the crack at any time is indicated by the circled lattice points. For this loading function, the fracture criterion used was met at relatively late times after the shock front has passed, so that the effect of crack growth on the transmitted wave is probably not large. These and other effects, such as material slippage, will be examined through comparisons of recorded time histories for Case 2 and Case 3 in forthcoming analyses.

4. DYNAMIC GRIFFITH CRITERION AND CRACK PROPAGATION

To improve the physical significance of the numerical solutions, the conclusion was reached that a more realistic, dynamic criterion for predicting and following the course of crack propagation in flawed, jointed, brittle media should be incorporated in the numerical method. A necessary step in making such a formulation change is to check the new code through comparisons with analytical results from some model problems, as will be discussed in Section 5.

The modifications needed to follow crack propagation are threefold. These are the logic associated with the crack geometry and crack propagation, the velocity threshold criterion, chosen here to be the Griffith criterion, and the velocity orientation criterion, chosen to be the direction transverse to the maximum principal stress vector. Programming of this formulation is currently underway.

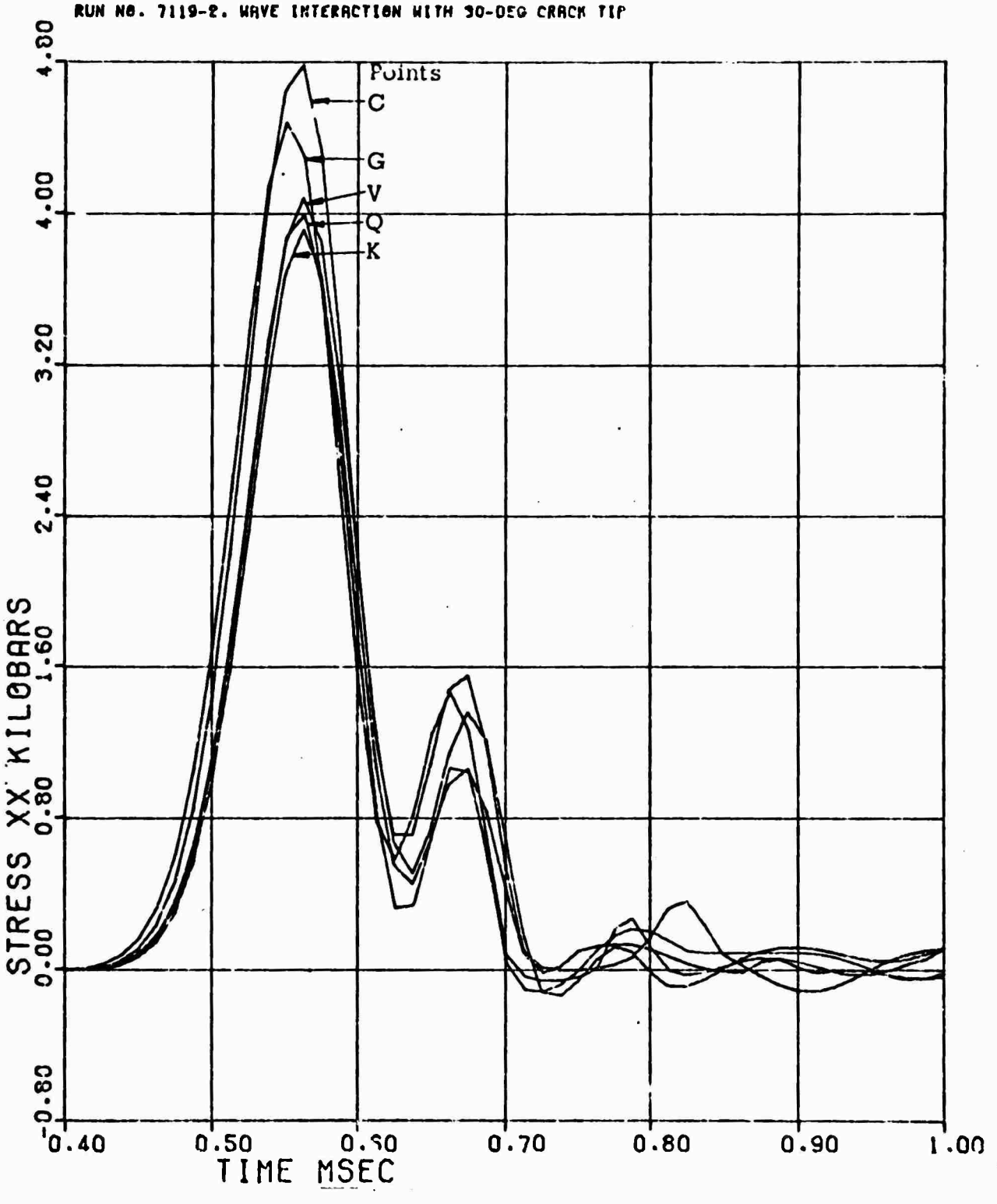

Figure 36. Stress (σ_x) Profiles at Points Along the Vertical Plane at $x \approx 300$ cm, Case 2.

Figure 36. Here the stress level is reduced at points above as well as below the crack tip. Time histories of the shear stress (σ_{xy}) at points along the vertical plane through the crack tip are shown in Figure 37.

3.5 CASE 3 - INTERACTION OF STRESS WAVE WITH SINGLE, FINITE-LENGTH CRACK, WITH CRACK GROWTH

For this case, the same problem as in Case 2 was solved, but with the provision in the code for permitting growth of the crack activated, as described previously.

Representative results of this code solution, as shown by the particle velocity fields for times of .5, .6, .7, and .9 msec, are given in Figures 5 to 7 in the Summary, Section 2.3.1, and in Figure 38. Associated principal stress fields for times of .5 and .6 msec are shown in Figures 39 and 40. Propagation of the crack does occur for this loading; the extent of the crack at any time is indicated by the circled lattice points. For this loading function, the fracture criterion used was met at relatively late times after the shock front has passed, so that the effect of crack growth on the transmitted wave is probably not large. These and other effects, such as material slippage, will be examined through comparisons of recorded time histories for Case 2 and Case 3 in forthcoming analyses.

4. DYNAMIC GRIFFITH CRITERION AND CRACK PROPAGATION

To improve the physical significance of the numerical solutions, the conclusion was reached that a more realistic, dynamic criterion for predicting and following the course of crack propagation in flawed, jointed, brittle media should be incorporated in the numerical method. A necessary step in making such a formulation change is to check the new code through comparisons with analytical results from some model problems, as will be discussed in Section 5.

The modifications needed to follow crack propagation are threefold. These are the logic associated with the crack geometry and crack propagation, the velocity threshold criterion, chosen here to be the Griffith criterion, and the velocity orientation criterion, chosen to be the direction transverse to the maximum principal stress vector. Programming of this formulation is currently underway.

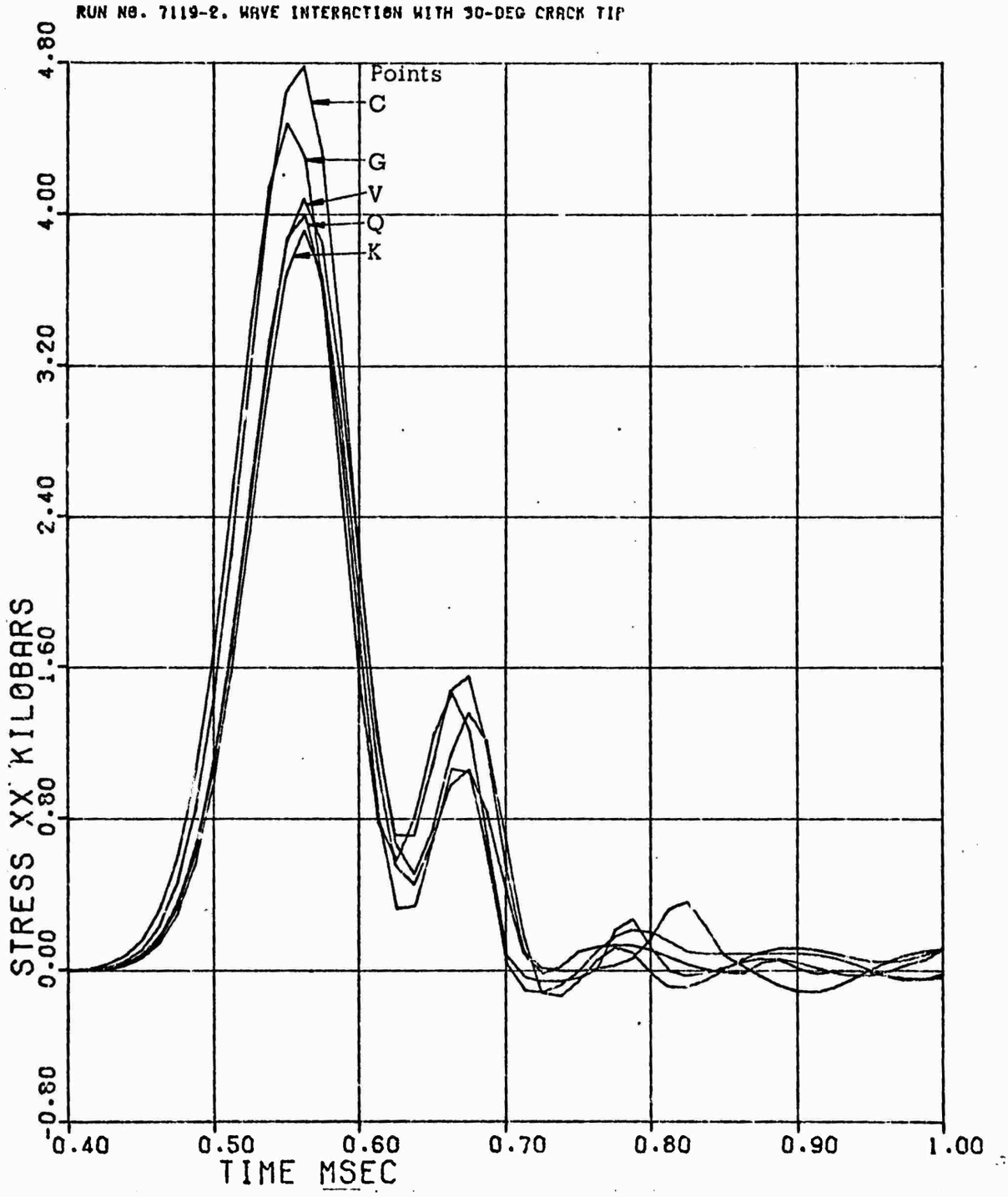

Figure 36. Stress (σ_x) Profiles at Points Along the Vertical Plane at $x \approx 300$ cm, Case 2.

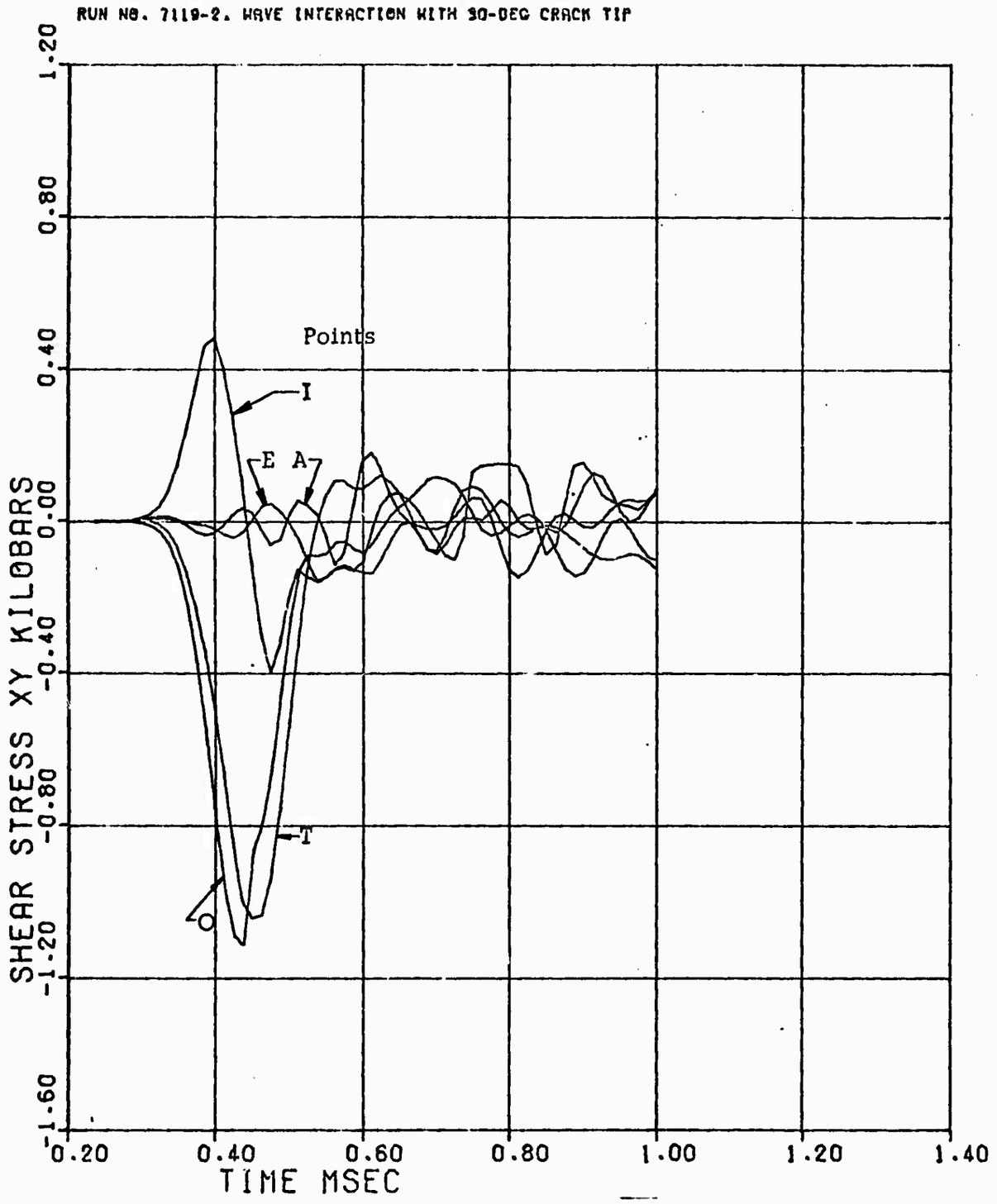

Figure 37. Shear Stress (σ_{xy}) Profiles at Points Along the Vertical Plane at $x \approx 200$ cm, Case 2.

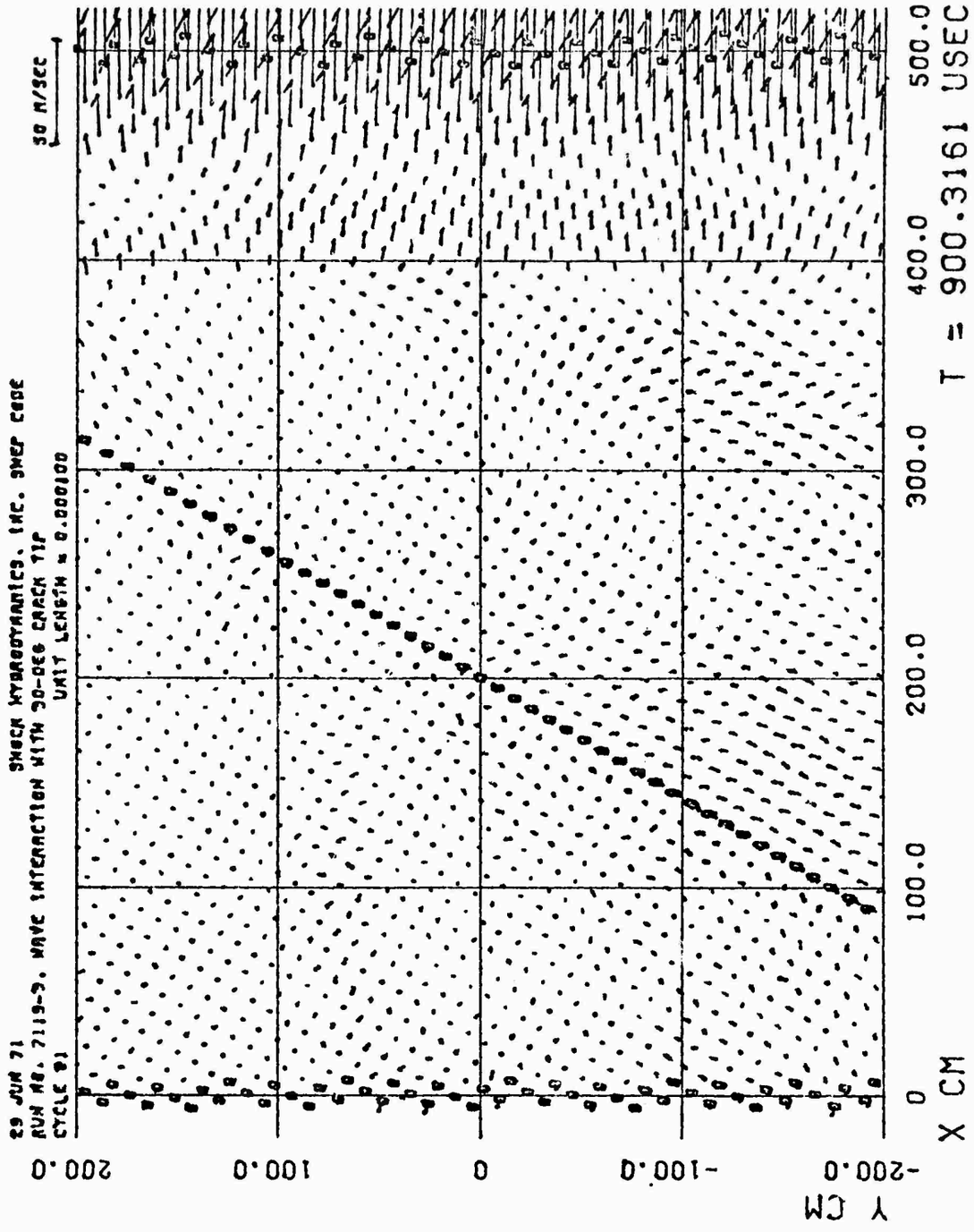

Figure 38. Particle Velocity Field, Case 3.

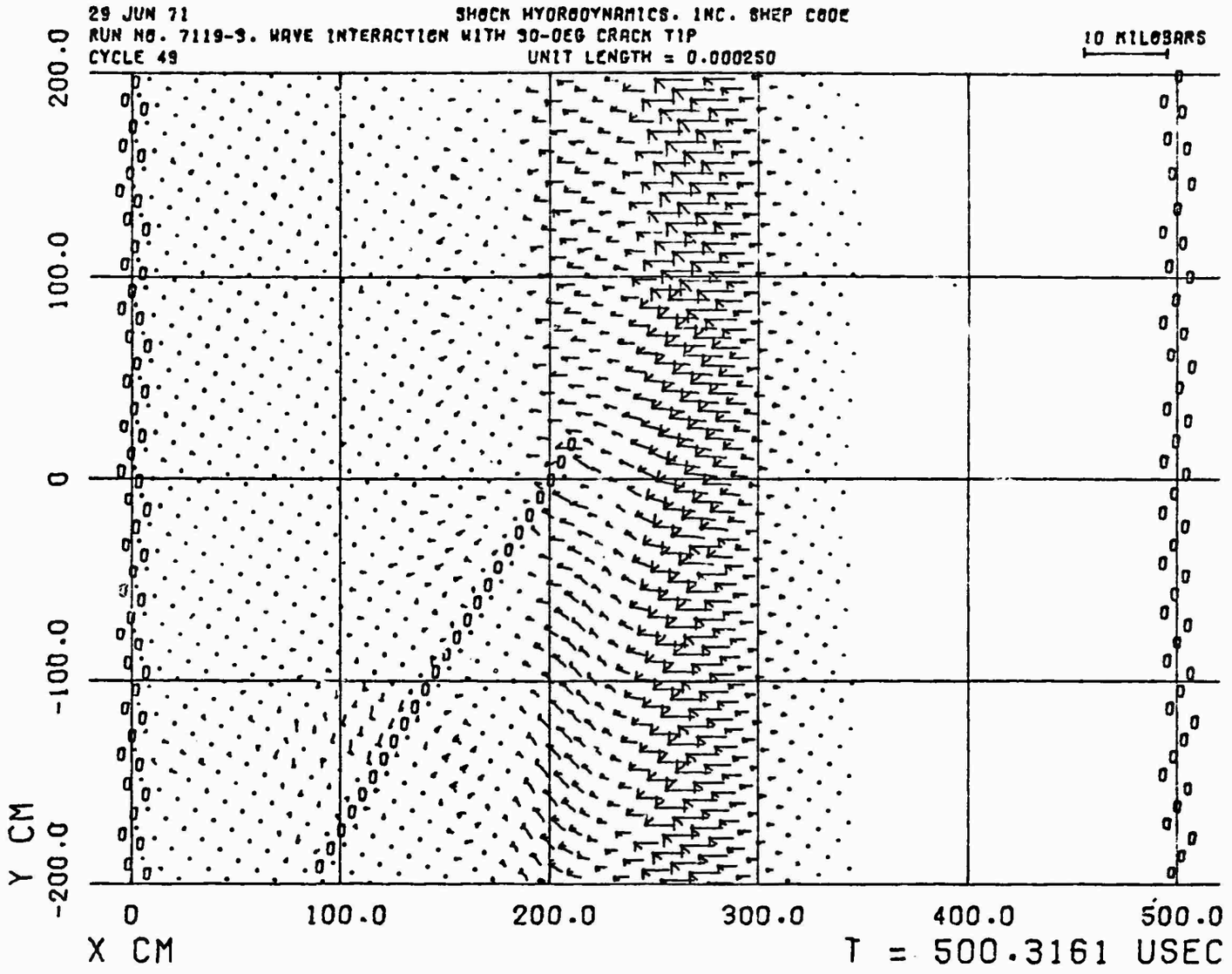

Figure 39. Principal Stress Field, Case 3.

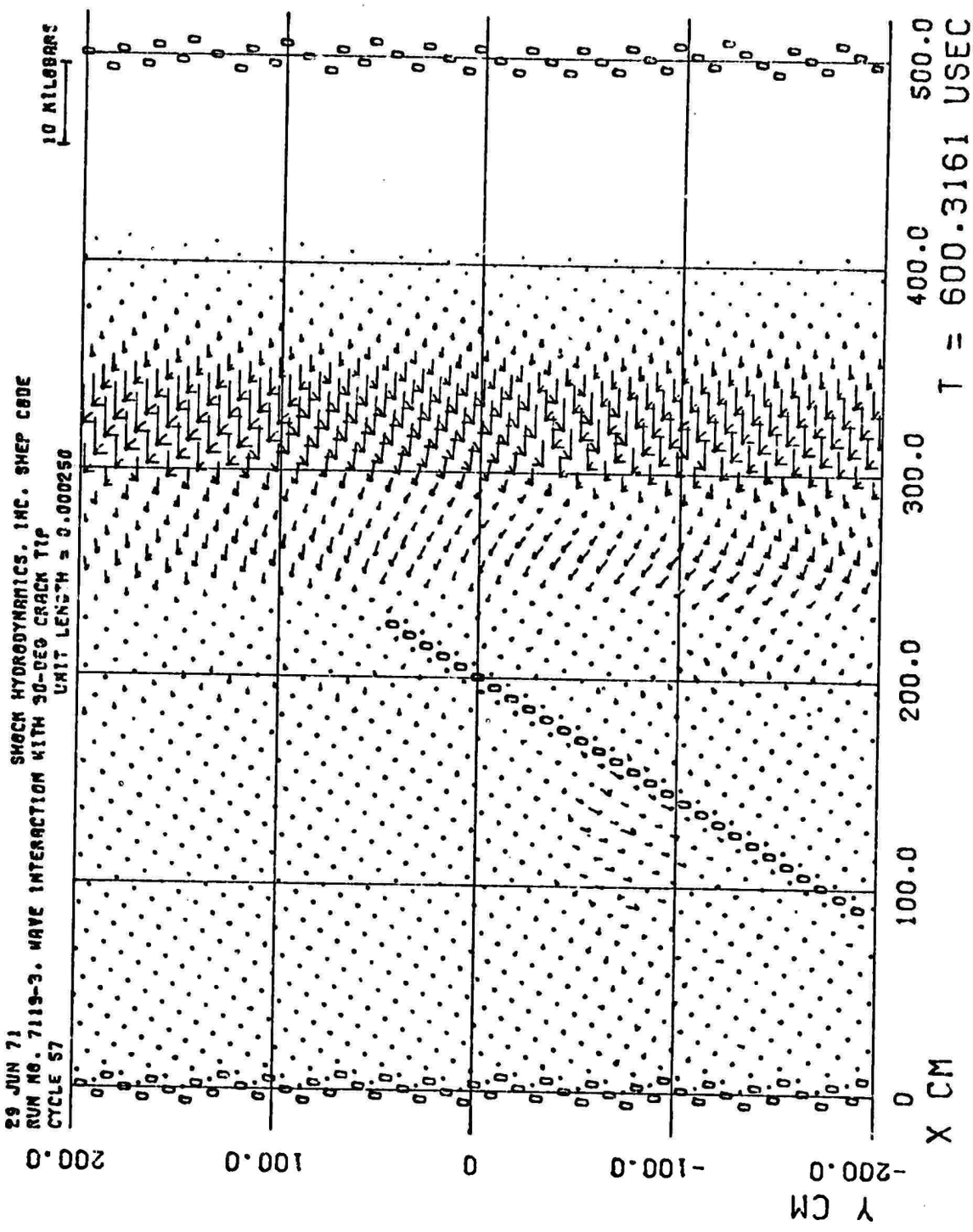

Figure 40. Principal Stress Field, Case 3.

It was suggested by Griffith that a useful way of accounting for controlled crack growth in an elastic body is to balance the rate of work (power input) to the body by the rate of uptake of strain energy, kinetic energy, and surface energy, i.e.,

$$P = \dot{U}_1 + \dot{U}_2 + \dot{U}_3 \tag{4}$$

where

$$P = \oint t_{ij} v_j \, d a_i \tag{5}$$

$$U_1 = \int W \, d V_o \tag{6}$$

$$U_2 = \frac{\rho_o}{2} \int v_k v_k \, d V_o \tag{7}$$

$$U_3 \approx \Gamma \oint n_k \, da_k \tag{8}$$

W is the strain energy density, Γ is the specific surface energy, a material constant, and the dots denote material differentiation. The material derivatives consist of two components, i.e.,

$$\dot{f} = \frac{\partial f}{\partial t}\Big|_{\vec{X}, \delta} + \frac{\partial f}{\partial \delta}\Big|_{\vec{X}, t} \dot{\delta} \tag{9}$$

where δ is a measure of the crack length. When the crack is not moving $\dot{f}$ is the ordinary material derivative.

In order to accommodate the crack motion it is necessary to follow this procedure. At each point in time, a test iteration is carried out in which the crack is assumed to run a small distance. New $\{U_1, U_2, U_3\}$ are calculated for the new δ, and Eqn. (4) is entered and checked. If the right hand side is less than the left hand side, the crack either has not yet started to run or the assumed increase in δ was too large. We propose to choose a small enough value of δ, such that the error incurred by always assuming the crack has not run when the inequality occurs, is a tolerable error. When equality occurs, the crack is advanced another small increment, and the program continues.

At each stage the program will calculate the direction of the principal maximum stress vector and the crack will move in a direction transverse to that. The crack geometry will be coded entirely like a free surface with the same boundary type characterization that is currently being used.

5. ANALYTICAL COMPARISON PROBLEMS

The only elasto-dynamic solutions that are currently available for an accelerating crack are those of Kostrov[7], Eshelby[8], and Achenbach[9]. The crack growth is produced by anti-plane shear. It was thus decided to modify the SHEP code to accommodate anti-plane shear or out-of-plane displacement in a manner that would retain the feature that the out-of-plane displacement remains independent of the z-coordinate (or θ-coordinate for the axisymmetric case). Thus, the additions maintain the two-dimensional character of SHEP because the out-of-plane motion merely superimposes on and does not couple with the in-plane motion, assuming that we are confined to the linear elastic region.

The additional equations that have been incorporated into the SHEP code to account for out-of-plane motion are shown below in differential form. The difference forms follow the same format as used by the rest of SHEP. We have

$$\frac{\partial \tau_{xz}}{\partial x} + \frac{\partial \tau_{yz}}{\partial y} + \frac{\tau_{yz}}{y}\Big|^{*} = \rho \dot{w} \tag{10}$$

$$\dot{E} = -(P+q)\,\dot{V} + V\,(s_x \dot{e}_x + s_y \dot{e}_y + s_\theta \dot{e}_\theta + \tau_{xy}\,\dot{e}_{xy} + \tau_{xz}\,\dot{e}_{xz} + \tau_{yz}\,\dot{e}_{yz}) \tag{11}$$

$$\tau_{xz} = G\,\dot{e}_{xz} \tag{12}$$

$$\tau_{yz} = G\,\dot{e}_{yz} \tag{13}$$

$$\dot{e}_{xz} = G\,\frac{\partial \dot{w}}{\partial x} \tag{14}$$

$$\dot{e}_{yz} = G\,\frac{\partial \dot{w}}{\partial y} \tag{15}$$

All the rest of the equations retain the same form (the form of the Jauman-Oldroyd derivatives is given in the Appendix).

A test problem consisting of simple shear motion of a slab has already been successfully run with the modified code, as discussed in the Appendix. The next case that will be run involves the loading of a stationary crack in anti-plane shear.

REFERENCES

1. N. B. Brooks and R. L. Lansdale, SHAPE-II Code, Hardening Technology Studies-III, Space and Missile Systems Organization, SAMSO-TR-68-69 (1968).

2. M. L. Wilkins, Calculation of Elastic-Plastic Flow, Lawrence Radiation Laboratory, Livermore, UCRL-7322, Rev. I (1969).

3. M. H. Wagner, Analytical Studies of Penetration Mechanics, Shock Hydrodynamics, 3030-2020FR (1969).

4. M. H. Wagner, Analytical Studies of Projectile Design and Performance, Shock Hydrodynamics, 7584-06 (1971).

5. M. H. Wagner and N. A. Louie, HARD HAT/PILE DRIVER Ground Motion Calculations, Space and Missile Systems Organization, SAMSO-TR-69-47 (1969).

6. M. H. Wagner, Shock Conditioned Behavioral Model for Granite, Defense Nuclear Agency, DASA-267C (1971).

7. B. V. Kostrov, "Unsteady Propagation of Longitudinal Shear Cracks," Prikl. Mat. i. Mek. 30, (English translation), 1241 (1966).

8. J. D. Eshelby, "The Elastic Field of a Crack Extending Non-Uniformly Under General Anti-Plane Loading," J. Mech. Phys. Solids 17, 177 (1969).

9. J. D. Achenbach, "Extension of a Crack by a Shear Wave," ZAMP 21, 887 (1970).

APPENDIX

CORRECTION TO THE ROTATIONAL TERM IN THE STRESS CALCULATIONS

During the examination of the formulation of the code preparatory to making the modifications discussed in Sections 4 and 5 of the report, an error in the sign of the rotational correction term in the stress calculations, as originally proposed by Wilkins[A1], was discovered. In addition, from the standpoint of material objectivity[A2], the form of the rotational term is seen to be written in only an approximate form. These statements are documented below. The sign was corrected in our code and a check of the correction was made by running a model problem. The results confirmed the sign correction and, in addition, verified the accuracy of the SHEP code.

In SHEP, the constitutive equations are correctly* subsumed in the form[A3]:

$$t_{ij} = s_{ij} - \delta_{ij} P(J) \tag{A1}$$

$$\hat{s}_{ij} = 2G\left(\dot{e}_{ij} - \frac{1}{3}\dot{\theta}\delta_{ij}\right) \tag{A2}$$

$$\theta = \ell n J \tag{A3}$$

$$J = \frac{dV}{dV_o} \tag{A4}$$

where

t_{ij} is the cartesian Couchy stress tensor

s_{ij} is the stress deviator tensor

P is the pressure

J is the local volume ratio, equal to the square root of the third stretch invariant.

---

*The term "correctly" implies that Eqn. (A2) satisfies the principle of material objectivity.

G is the shear modulus

θ is the dilatation

$\dot{e}_{ij}$ is the Cartesian strain rate tensor

V is the local instantaneous specific volume

and in (A4), $\frac{d}{dV_o}$ is the particle-differentiator.

From Eqn. (A3) and (A4), it follows that

$$J = \frac{\dot{V}}{V} \tag{A5}$$

Furthermore in Eqn. (A2), the dot over $\dot{e}_{ij}$ denotes the material derivative while the hat over s_{ij} denotes the Jaumann-Oldroyd derivative. The form of the latter is given by:

$$\hat{s}_{ik} = \dot{s}_{ik} - v_{i,j}\, t_{jk} + t_{ij}\, v_{j,k} \tag{A6}$$

where

$$v_{i,j} = \dot{e}_{ij} + \omega_{ij} \tag{A7}$$

or

$$\frac{v_{i,j} + v_{j,i}}{2} = \dot{e}_{ij} \tag{A8}$$

where

ω_{ij} is the spin tensor.

The last two terms on the right hand side of Eqn. (A6) correspond to Wilkins' δ_{ij}; a simple calculation reveals that the entire form of Eqn. (B-14) on page 78 of Reference A1 is formally incorrect but approximately appropriate (apart from a sign error).

The sign error apparently arose in the following way: Wilkins introduces an angular velocity vector, which he denotes by [sin $\dot{\omega}$]. The angular velocity vector is correctly taken as the curb of the velocity vector which, according to the usual <u>right-handed</u> correction, corresponds to a <u>counter-</u>

clockwise rotation. Wilkins then uses the rotation angle ω to transform the stress components to new rotated components. The transformation equations he adopts are taken from Timoshenko[A3]. Presumably Wilkins changed the signs of the terms that are odd in ω, because Timoshenko shows a diagram in which the rotation is clockwise. What one must notice, however, is that Timoshenko's picture is based on a left-handed system of axes. Thus Timoshenko's equation should have been subsumed without the sign change.

To further check our logic, we ran the following simple problem. A slab is set into simple shear motion, of:

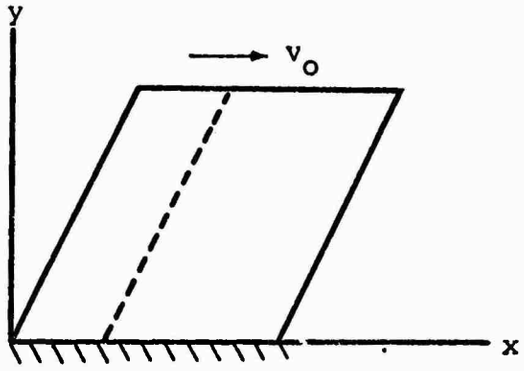

Nonlinear (Poynting) effects are associated with the lengthening of the originally upright fibers. The correct rotation terms (with the right sign) predict a tensile stress in the lengthened fibers, in agreement with the analytical solution. The original program, with the incorrect sign, predicts compression. Keep in mind that these are second order stresses and thus the effect of this error on the overall computation becomes important only when the first order stresses are comparable to the shear modulus of the material. The reason is that the second-order stresses go as the square of the first-order stresses, e.g., in the shear problem:

$$\frac{\sigma_y}{G} \sim \left(\frac{\tau_{xy}}{G}\right)^2 \qquad \text{(A9)}$$

In the process of making these changes in SHEP, we checked out a model problem, namely the simple shear at constant velocities of an infinitely long slab (a 1-D problem). The results, in terms of the stress at the moving

surface and the stress at the fixed surface are plotted in Figures A1 and A2, respectively. The analytical solution is just a sum of Heaviside step functions. The agreement with the analytical solution is attested to by the fact that the computed jumps fall directly (within 1%) on the grid line (both coordinate axes are non-dimensionalized). The general solution looks like

$$-\frac{\tau_{xy}}{M_o G} = \sum_{n=0}^{\infty} [H(s-y-2nh] + H(s+y-2h-2nh)] \qquad (A10)$$

where

M_o (the Mach number) $= \frac{v_o}{c}$

$s = ct$

$c = \sqrt{\frac{G}{\rho}}$

and h is the height of the slab.

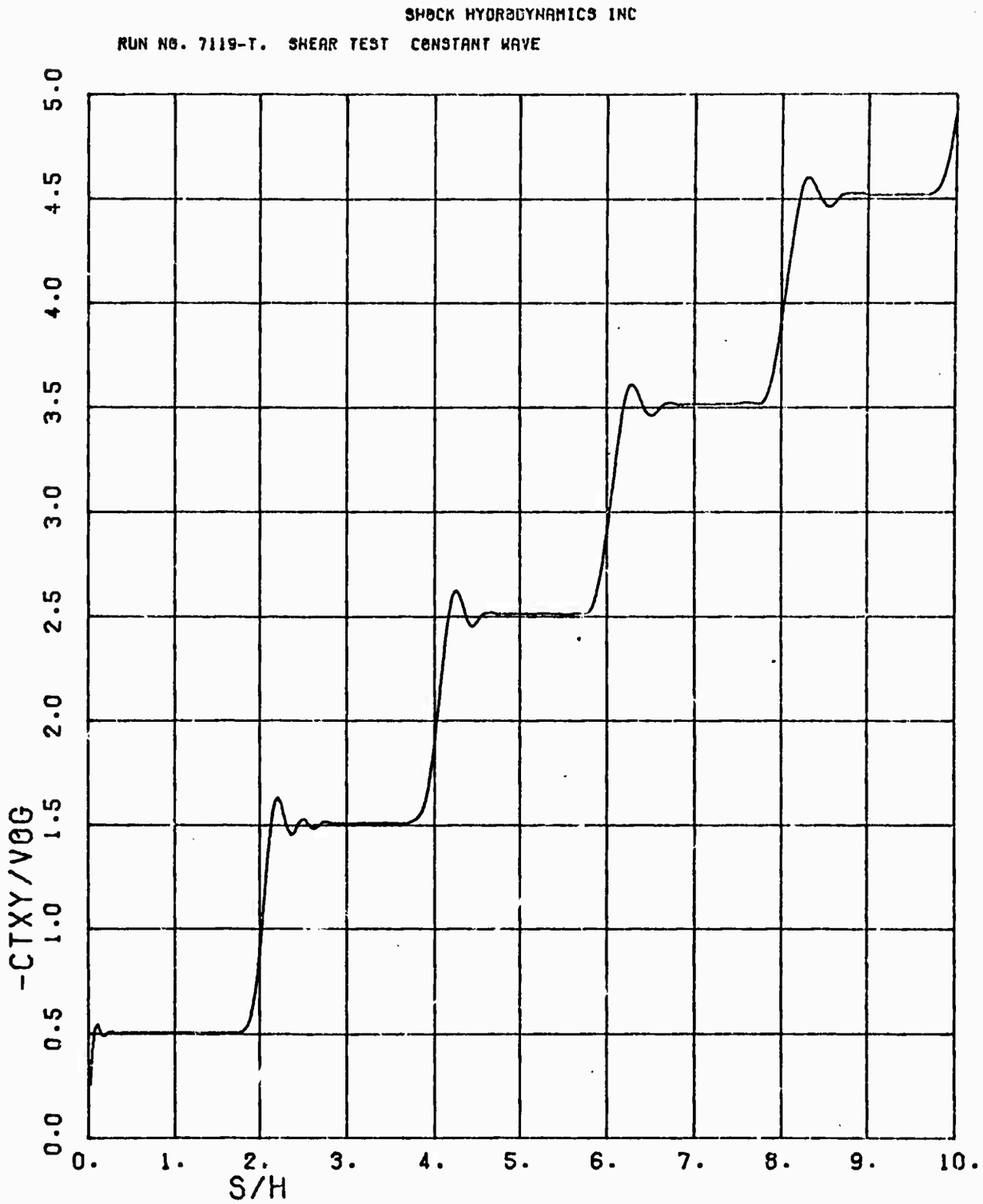

Figure A1. Shear Stress at the Moving Surface

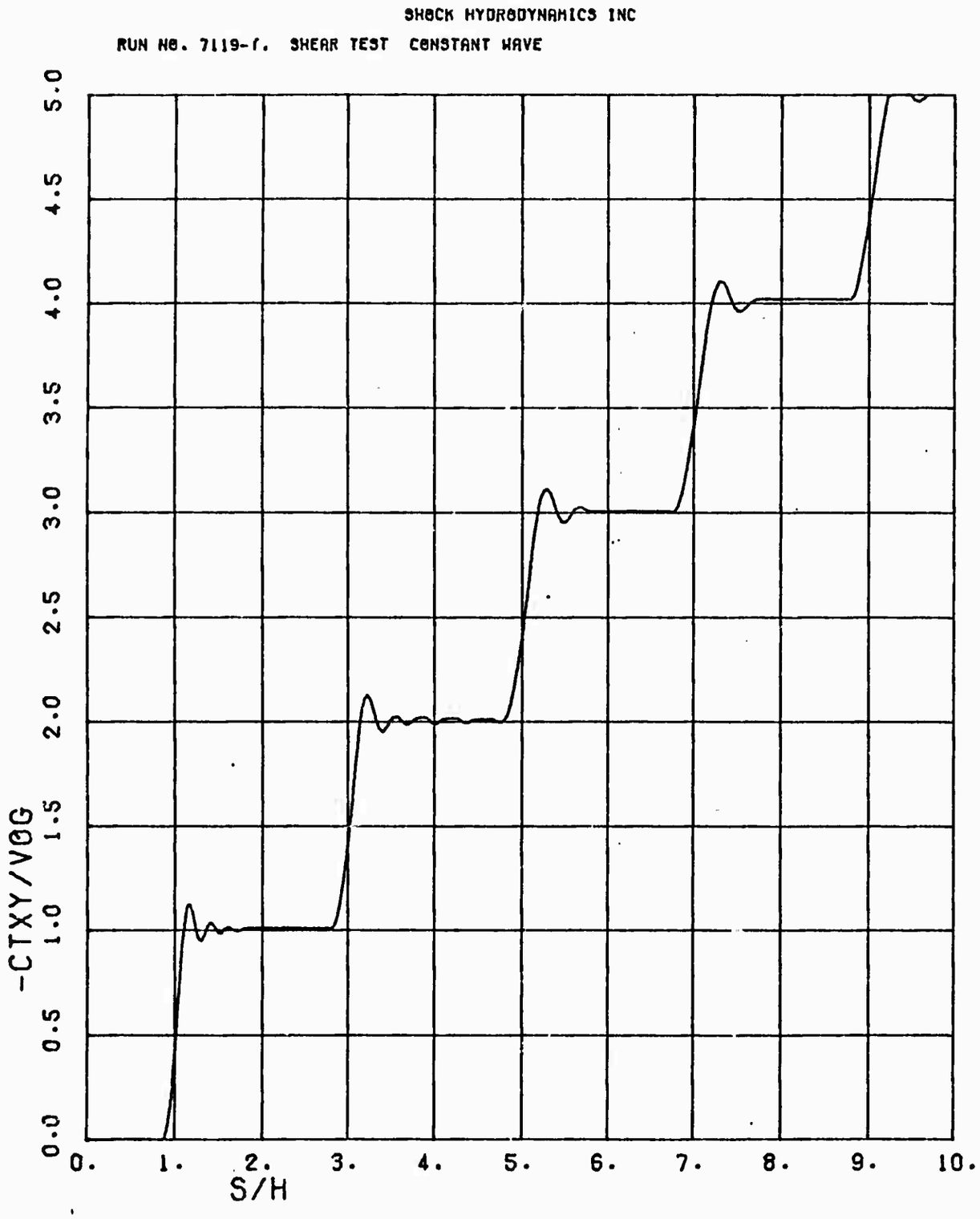

Figure A2. Shear Stress at the Clamped Surface

REFERENCES

A1. M. L. Wilkins, Calculation of Elastic-Plastic Flow, Lawrence Radiation Laboratory, Livermore, UCRL-7322, Rev. I (1969).

A2. A. C. Eringen, "Nonlinear Theory of Continuous Media," McGraw-Hill, New York (1962).

A3. S. Timoshenko and J. N. Goodier, "Theory of Elasticity," McGraw-Hill, New York (1951).